Elastic and inelastic scattering of electrons by nuclei

V. K. Luk'yanov* and Yu. S. Pol'**

*Joint Institute for Nuclear Research, Dubna

**P. N. Lebedev Physics Institute, Moscow

Fiz. El. Chast. Atom. Yad., 5, 955-1022 (October-December 1974)

A review is presented of the present status of theoretical methods and of the principal results of their application to elastic and inelastic scattering of electrons by nuclei with excitation of low-lying collective status in the nuclei. The advantages and shortcomings of phenomenological methods and model-independent methods for analyzing the experimental data are considered. The possibilities are demonstrated of directly describing the data within the framework of the independent-particle model, of the α-cluster model, of approaches with allowance for the short-range correlations in the nuclei, and of the macroscopic and microscopic nuclear models.

INTRODUCTION

Interest in the study of nuclear structure with the aid of elastic and inelastic scattering of electrons has been renewed of late. The reason is the appearance of accurate data on the scattering by a number of nuclei at different energies and at large momentum transfer, up to $q \sim 3.5$ F^{-1}, investigation of isotopic differences in the charge-density distributions, attempts at jointly studying elastic and inelastic form factors, and new data on quasielastic proton knock-out from deep shells of the nucleus and on the giant dipole resonance, and other factors (a detailed bibliography up to 1970 is given in ref. 1). Notice should also be taken of the development of the corresponding theoretical methods, such as the model-independent analysis of form factors, calculations of ground states of nuclei by the Hartree–Fock method, etc.

Compared with the scattering of nuclear particles, the electromagnetic character of the interaction of electrons with nuclei greatly simplifies interpretation of the experimental data. They are also preferable to photonuclear reactions, since they make it possible to vary, more or less independently, the energy and momentum transferred to the nucleus. This makes it possible to assess, e.g., the distribution of the charge in the nucleus in those characteristic regions that are responsible for nuclear transitions to excited states.

In this paper we consider the principal theoretical approaches used to extract information on the structure of the nucleus from data on electron scattering, and methods of directly calculating the form factors within the framework of the most typical nuclear models and schemes. We limit outselves to the study of only electric form factors for elastic and inelastic scattering with transition of the nucleus to the lowest collective-excitation states.

1. HIGH-ENERGY APPROXIMATION

In problems where electrons for the corresponding form factors or cross sections are used to study the nucleus, it is convenient to use as simple expressions as possible. This explains the physical principles of the phenomenon and, what is of practical importance, permits the performance of the many repeated calculations needed to fit the parameters of the nuclear models or schemes chosen for comparison with experiment. From this point of view, a method based on numerical solution of the Dirac equation to find the scattering phase shifts, followed by summation of the partial amplitudes, which is traditionally called the phase-shift analysis method, is inconvenient. The difficulties of this approach include also the need for attaining high accuracy in calculation of the Coulomb potential from the specified charge density of the nucleus and with the need for summing an alternating-sign series of partial amplitudes (quantities on the order of unity) in order to find exponentially small cross sections at large momentum transfers.

In this respect, the simplest is the plane-wave Born approximation. Practical experience has shown that this method can be used with assurance for light nuclei with $Z \leq 6$ in the entire presently accessible experimental region of momentum transfers, with the exception of the points where the cross sections are minimal. As to medium and heavy nuclei, it is possible to take into account here the distortions of the incident and outgoing waves in the Coulomb field of the nucleus. A sufficiently accurate quantitative method for taking these distortions into account can be developed without resorting to the exact phase-shift analysis method, by using the so-called high-energy approximation.

We present below a methodological comparison of these three methods, but we give first the fundamental initial expression for the electron elastic and inelastic scattering cross sections and the high-energy approximation. These expressions are not only convenient for particular numerical calculations, but are quite illustrative and reduce to the well-known Born approximation in the particular case when there is no distortion.

Theoretical Methods in High-Energy Electron Scattering

To study the details of nuclear structure it is necessary that the wavelength of the electron be smaller than the dimensions of the nucleus, i.e., $kR \gg 1$. The most instructive in this case is the cross section for scattering through angles $\vartheta \gg (kR)^{-1}$, where there are characteristic minima and maxima. Their positions and forms depend strongly on the nuclear structure. Within the framework of these conditions $kR \gg 1$, $E \gg V$, the high-energy approximation is the most appropriate for our problem. The initial conditions yield expressions of somewhat different form for the scattering amplitude. This question was analyzed in detail in ref. 2. We present here a brief listing of the methods, based on a general expression for the amplitude in the form

$$f(q, E) = \frac{E}{2\pi} \int g(\mathbf{r} v_i v_f) \exp\{i[\mathbf{qr} + \phi(\mathbf{r})]\} V(\mathbf{r})\, d\mathbf{r}, \qquad (1)$$

where g and ϕ are the distorting amplitude and phase functions; v_i and v_f are free spinors, and the Coulomb potential is connected with the charge-density distribution by

$$V(\mathbf{r}) = -Ze^2 \int \frac{\rho(\mathbf{x})\, d\mathbf{x}}{|\mathbf{r}-\mathbf{x}|}. \tag{2}$$

It is obvious that the Born approximation is obtained from (1) by putting

$$g = v_f^\dagger v_i; \quad \phi(\mathbf{r}) = 0. \tag{3}$$

The amplitude function g and the phase function ϕ depend on the concrete utilization of the high-energy approximation conditions. Thus, the usual eikonal approach yields

$$g = v_f^\dagger v_i; \quad \phi = -\frac{E}{k}\int_0^\infty V(\mathbf{r} - \hat{k}_i s)\, ds. \tag{4}$$

Then, confining ourselves to small scattering angles $\vartheta \ll (kR)^{-1}$ and to the assumption that the trajectory is linear, we can reduce the amplitude to the following integral:[3]

$$f_E = -ik(v_f^\dagger v_i)\int_0^\infty J_0(k\rho\vartheta)\left\{\exp\left[-i\frac{E}{k}\int_0^\infty V(\rho + \hat{k}z)\, dz\right] - 1\right\}\rho\, d\rho. \tag{5}$$

Methodological calculations performed on the basis of this equation for the cross sections for scattering of electrons by nuclei with a step-like charge-density distribution have shown[4] that the phase function ϕ and the preexponential factor g must be determined with greater accuracy. The factor g must take into account the distortion of the front of the electron wave by the Coulomb field in the region of the nucleus. Such a factor was introduced artificially in ref. 4, but the method has not found use in comparison with experiment.

Another approach was proposed in ref. 5, where asymptotic summation of the Born series yielded

$$g = v_f^\dagger v_i; \quad \phi = -\frac{E}{k}\left[\int_0^\infty V(\mathbf{r} - \hat{k}_i s)\, ds + \int_0^\infty V(\mathbf{r} + \hat{k}_f s)\, ds\right], \tag{6}$$

which is valid at large scattering angles $\vartheta > (kR)^{-1/2}$. In this case, on going over to linear trajectories, the expression for the amplitude (1) becomes explicitly definite. In comparison with (4), we have here an additional term in the phase shift and this term, roughly speaking, takes into account the distortion of the wave function of the electron on its path from the nucleus to $+\infty$. Although methodological calculations on the basis of this approach,[6] when compared with the exact phase-shift analysis methods, result in agreement between the positions of the minima and maxima of the angular distribution, the phase-shift-analysis cross sections turn out to be 10-15% higher and this again appears to be due to inaccuracy in determination of the preexponential factor g.

The most successful form of the amplitude was proposed in ref. 7 specially for the case of scattering through large angles $\vartheta > (kR)^{-1}$:

$$g = u_f^\dagger(\mathbf{r})\, u_i(\mathbf{r});$$

$$\phi = -\frac{E}{k}\left[\int_0^\infty U(\mathbf{r} - \hat{k}_i s)\, ds + \int_0^\infty U(\mathbf{r} + \hat{k}_f s)\, ds\right], \tag{7}$$

where $u_{i,f}(\mathbf{r})$ are obtained from the quasiclassical solution of the Dirac equation for the wave functions with respect to the electron motion:

$$\Psi^{(\pm)}(\mathbf{r}, \mathbf{k}) = u^{(\pm)}(\mathbf{r}, \mathbf{k})\exp\left[i\mathbf{kr} - i\frac{E}{k}\int_0^\infty U(\mathbf{r} \mp \hat{k}s)\, ds\right]. \tag{8}$$

To justify the initial expression (1) with functions g and ϕ in the form (7), the authors of ref. 7 have had to arbitrarily subdivide the Coulomb potential V into two parts, a smooth part U containing the lower Fourier components of the potential, which make the main contribution to scattering through small angles $\vartheta < (kR)^{-1}$, and the high-frequency component v, responsible for scattering through large angles $\vartheta > (kR)^{-1}$. Then, using the well-known expression for the transition matrix in the case of two potentials

$$T_{if} = \langle \Psi_f^{(-)}(U) \,|\, v \,|\, \chi_i^{(+)}(V)\rangle + \langle \Psi_f^{(-)}(U) \,|\, U \,|\, \exp(i\mathbf{kr})\rangle, \tag{9}$$

it is possible to neglect the contribution of the second term to the amplitude at angles $\vartheta > (kR)^{-1}$, and in the first term it is possible, as usual, to replace the exact solution $\chi^{(+)}$ by the wave $\Psi^{(+)}$ distorted in the potential U. Similar arguments make it possible to replace in the obtained expression the potential v by the total Coulomb potential V, since its low-frequency part U is in essence automatically cut off upon integration with the strongly oscillating functions (8) in the investigated region of angles $\vartheta > (kR)^{-1}$. As a result we have

$$f_{HE}(q, E) = \frac{E}{2\pi}\int u_f^\dagger(\mathbf{r})\, u_i(\mathbf{r})\exp\left[i\mathbf{qr} - i\frac{E}{k}\int_0^\infty U(\mathbf{r} - \hat{k}_i s)\, ds - i\frac{E}{k}\int_0^\infty U(\mathbf{r} + \hat{k}_f s)\, ds\right] V(\mathbf{r})\, d\mathbf{r}. \tag{10}$$

The authors of ref. 7 have calculated the amplitudes (10) for the potential V with a step-function charge density distribution $\rho = \theta(\mathbf{r} - \mathbf{R})$. In this case the cross section is expressed by an analytic equation and agrees well with the corresponding exact calculation by the phase-shift-analysis method.

Further development of this method for a realistic form of a Fermi density $\rho_F(r)$ and for an arbitrary form of the charge-density distribution was carried out in refs. 8 and 9, where a concrete comparison with the phase-shift analysis has demonstrated its extensive capabilities and the good accuracy for numerical calculations and for comparison with experiment.

Differential Elastic and Inelastic Scattering Cross Sections

We write down the electron scattering cross section in the general form

$$\frac{d\sigma}{d\Omega} = \sigma_{i\to f}(\vartheta) = \frac{E^2}{(2\pi)^2}\cdot\frac{1}{2}\cdot\frac{1}{2J_i+1}\sum_{\sigma_i\sigma_f}\sum_{M_iM_f}|T_{if}|^2. \tag{11}$$

The matrix element of the transition from the initial (i) to the final (f) state will be represented in the form

$$T_{if} = \langle J_f M_f | \int d\mathbf{r} \Psi_f^{(-)+}(\mathbf{r}) V(\mathbf{r}\xi) \Psi_i^{(+)}(\mathbf{r}) | J_i M_i \rangle. \quad (12)$$

The wave function of the nuclear state $|JM\rangle$, which depends on the corresponding coordinate ξ of internal motion, is determined within the framework of some model of the nucleus. The Coulomb interaction of the electron with the nucleus is given by

$$V(\mathbf{r}\xi) = -Ze^2 \int \frac{\rho(\mathbf{x}\xi)\, d\mathbf{x}}{|\mathbf{r}-\mathbf{x}|}. \quad (13)$$

Neglecting the electron energy loss $\Delta E \ll E$, i.e., assuming $k_i = k_f$, we write within the framework of the high-energy approximation

$$\Psi_f^{(-)+}\Psi_i^{(+)} = g(\mathbf{r}v_f^+v_i)\exp[i\mathbf{q}\mathbf{r} + i\phi(\mathbf{r})], \quad (14)$$

where g and ϕ are given in (7).

Now, making the change of variable $\mathbf{u} = \mathbf{r} - \mathbf{x}$ and using the expansions

$$\left.\begin{aligned} g(\mathbf{u}+\mathbf{x},\ v_f^+v_i) &= g(\mathbf{x},\ v_f^+v_i) + \ldots; \\ \phi(\mathbf{u}+\mathbf{x}) &= \phi(\mathbf{x}) + \nabla_u\phi(\mathbf{u}+\mathbf{x})|_{u=0}\mathbf{u} + \ldots, \end{aligned}\right\} \quad (15)$$

we obtain

$$T_{if} = -4\pi Ze^2 \int d\mathbf{x} \frac{g(\mathbf{x}v_f^+ v_i)}{q_{\text{eff}}^2(\mathbf{x})} \times \exp\{i[\mathbf{q}\mathbf{x} + \phi(\mathbf{x})]\}\langle J_f M_f | \rho(\mathbf{x}\xi) | J_i M_i \rangle, \quad (16)$$

where

$$q_{\text{eff}}(\mathbf{x}) = \mathbf{q} + \nabla_u\phi(\mathbf{u}+\mathbf{x})|_{u=0}. \quad (17)$$

Substituting here $\rho(\mathbf{x}\xi)$ in the form of the expansion

$$\rho(\mathbf{x}\xi) = \sum_{LM} \mathcal{P}_{LM}(x\xi) Y_{LM}^*(\hat{x}) \quad (18)$$

and using the Wigner–Eckart theorem (L is an integer)

$$\langle J_f M_f | \mathcal{P}_{LM} | J_i M_i \rangle = (J_i L M_i M | J_f M_f)\langle J_f \| \mathcal{P}_L \| J_i \rangle, \quad (19)$$

we obtain

$$\langle J_f M_f | \rho(\mathbf{x}\xi) | J_i M_i \rangle = \sum_{LM} \rho_L(x) Y_{LM}^*(\hat{x})(J_i L M_i M | J_f M_f), \quad (20)$$

where

$$\rho_L(x) = \langle J_f \| \mathcal{P}_L(x,\ \xi) \| J_i \rangle \quad (21)$$

will be called the radial transition density of the nucleus. Substituting (16) and (20) in the equation for the cross section (11) and recognizing that in the high-energy approximation we have[2]

$$g(\mathbf{x},\ v_f^+v_i) = g(\mathbf{x})v_f^+v_i,$$

we obtain a final expression for the cross section:

$$\sigma_{i\to f} = \sigma_{\text{Mott}} \frac{2J_f+1}{2J_i+1} \sum_{LM} \frac{1}{2L+1} |F_{LM}|^2, \quad (22)$$

where $\sigma_{\text{Mott}} = (2Ze^2/q^2)^2 \cos^2\vartheta/2$ is the Mott cross section; the form factor is

$$F_{LM} = q^2 \int d\mathbf{x} \frac{g(\mathbf{x})}{q_{\text{eff}}^2(\mathbf{x})} \exp\{i[\mathbf{q}\mathbf{x} + \phi(\mathbf{x})]\}\rho_L(x) Y_{LM}^*(\hat{x}). \quad (23)$$

Thus, the problem of calculating the scattering cross section breaks up into two independent parts, calculation of the radial transition density by means of Eq. (21) within the framework of the chosen nuclear model, and the calculation of the integrals using (23). The entire physical information on the structure of the nucleus is contained in the form factors F_{LM}, which will therefore be the principal object of the present research.

Calculation of the Form Factors in the High-Energy Approximation

The wave functions $\Psi^{(\pm)}(\mathbf{r}, \mathbf{k})$ of the relative motion of the electron, as solutions of the Dirac equation, were obtained in the high-energy approximation in ref. 8. Neglecting the electron mass, we express them in the form

$$\Psi^{(\pm)}(\mathbf{r},\ \mathbf{k}) = \frac{1}{2E}\left(1 - \frac{1}{4}\cdot\frac{U(\mathbf{r})}{E} \pm \frac{\hat{k}\nabla\phi^{(\pm)}(\mathbf{r},\ \mathbf{k})}{4E}\right)(\sigma\nabla S^{(\pm)}(\mathbf{r},\ \mathbf{k}) + E - U(\mathbf{r}))\, v\exp[iS^{(\pm)}(\mathbf{r},\ \mathbf{k})], \quad (24)$$

where

$$S^{(\pm)}(\mathbf{r},\ \mathbf{k}) = \mathbf{k}\mathbf{r} \mp \phi^{(\pm)}(\mathbf{r},\ \mathbf{k});\ \phi^{(\pm)}(\mathbf{r},\ \mathbf{k}) = \int_0^\infty U(\mathbf{r} \mp \hat{k}s)\, ds. \quad (25)$$

Following ref. 7, we can obtain an explicit expression for this function in the vicinity of the nucleus by expanding the potential V in a Taylor series. Then the smooth potential is

$$U(r) = V(0) + ak^3r^2/2. \quad (26)$$

In the calculation of (25) we assume that the trajectories are straight lines. Choosing then $0z \uparrow\uparrow \mathbf{k}$ and assuming $\mathbf{r} = \boldsymbol{\rho} + \hat{k}z$, where ρ is the impact distance, we obtain

$$\phi^{(\pm)}(\mathbf{r},\ \mathbf{k}) = -\int_0^z U(\sqrt{\rho^2+t^2})dt \pm \int_0^\infty [U(t) - U(\sqrt{\rho^2+t^2})]\, dt. \quad (27)$$

The first integral is evaluated directly following the substitution (26), and the second is obtained after expanding in powers of ρ^2 and retaining only the quadratic term. The intermediate steps, the expressions for (24), the form of the expansion coefficients, and also g, q_{eff}, and ϕ from (23) are given in Appendix 1. The latter depend on the chosen charge-density distribution in the nucleus.

We now consider the integrals (23), which are the form factors of the nucleus in electron scattering. When they are calculated it must be recognized that the region where the principal contribution is made for angles $\vartheta > (kR)^{-1}$ is the vicinity of the nucleus, where the expansion (26) is valid. If $\vartheta > (kR)^{-1}$, $qx \sim qR \gg 1$, one can use the method of asymptotic expansion in reciprocal powers of the quantity (qx) in the exponential of (23). We now choose $0z \uparrow\uparrow \mathbf{q}$ and put $\cos\hat{\mathbf{q}}\hat{\mathbf{x}} = \mu$. Then $d\mathbf{x} = -x^2 dx d\mu d\varphi$ and the corresponding integral with respect to $d\mu$ takes the form

$$I_{LM} = \int_{-1}^{1} \frac{g(x\mu\varphi)}{q_{\text{eff}}^2(x\mu\varphi)} \exp\{i[qx\mu + \phi(x\mu\varphi)]\}\rho_L(x) Y_{LM}(\mu\varphi)\, d\mu. \quad (28)$$

Using the identity

$$\exp\{i[qx\mu+\phi(x\mu\varphi)]\}^{\cdot}=\frac{1}{iqxD(x\mu\varphi)}\frac{\partial}{\partial\mu}\exp\{i[qx\mu+\phi(x\mu\varphi)]\},\quad(29)$$

where

$$D(x\mu\varphi)=1+\frac{1}{qx}\cdot\frac{\partial}{\partial\mu}\phi(x\mu\varphi),\quad(30)$$

we obtain after integrating by parts

$$I_{LM}=\sum_{\varepsilon}\varepsilon\frac{g(x\varepsilon)}{q^2_{\text{eff}}(x\varepsilon)}\left[\frac{1}{iqx}\sum_{\nu=0}^{L}\frac{i^\nu}{(qx)^\nu}\frac{\partial^\nu/\partial\mu^\nu Y_{LM}(\mu\varphi)}{D^{\nu+1}(x\mu\varphi)}\right]_{\mu=\varepsilon}$$
$$\times\exp\{i[qx\varepsilon+\phi(x\varepsilon)]\}+\left\{\frac{1}{(qx)^2}\left[\frac{\partial}{\partial\mu}\left(\frac{g(x\mu\varphi)}{q^2_{\text{eff}}(x\mu\varphi)\,D(x\mu\varphi)}\right)\right]_{\mu=\varepsilon}\right.$$
$$\left.\times\frac{Y_{LM}(\varepsilon\varphi)}{D(x\varepsilon\varphi)}\cdot\exp\{i[qx\varepsilon+\phi(x\varepsilon)]\}\right\}.\quad(31)$$

We can neglect here the second term, since it is of higher order than the first. Indeed, estimates yield for their ratio

$$\left(\frac{1}{q^2}\cdot\frac{Z}{137}\cdot\frac{1}{(kR)^2}\cdot\frac{1}{qR}\right)\Big/\left(\frac{1}{q^2}\cdot\frac{1}{qR}\right)=\frac{Z}{137}\cdot\frac{1}{(kR)^2},$$

which exceeds the accuracy of the high-energy approximation $V/E\sim(Z/137)(1/kR)$. In (31) we took into account the fact that at the points $\mu=\varepsilon=\pm1$ there is no longer a dependence on the azimuthal angle in the functions q^2_{eff} and ϕ (see Appendix 1) and this dependence remains only in $D(x\mu\varphi)$, in the form

$$qxD(x\mu\varphi)|_{\mu=\varepsilon}=A(x\varepsilon)+B(x\varepsilon)\cos^2\varphi.\quad(32)$$

The integration with respect to $d\varphi$ in (23) can then be carried out exactly (Appendix 2), and the form factor reduces to the one-dimensional integral

$$F_{LM}=2\pi iq\sum_{\varepsilon=\pm1}\varepsilon\int_0^\infty\frac{G_{LM}(x\varepsilon)}{q^2_{\text{eff}}(x\varepsilon)}$$
$$\times\exp\{i[qx\varepsilon+\phi(x\varepsilon)]\}\rho_L(x)\,x\,dx,\quad(33)$$

where

$$G_{LM}=G_0(x\varepsilon)\sum_{\nu=0}^{L}i^\nu\left[\frac{\partial^\nu}{\partial\mu^\nu}Y_{L0}(\mu)\right]_{\mu=\varepsilon}J^{(\nu)}_M(x\varepsilon);\quad(34)$$

$$J^{(\nu)}_{M=2m}(x\varepsilon)=\frac{1}{A^\nu}\sum_{n=0}^{m}(-1)^nC^{2m}_{2n}\frac{(2m-2n-1)!!\,(2n-1)!!}{2^m m!}$$
$$\times\left(1-\frac{B}{A+B}\right)^{m-n}\times F(m-n+1/2,\ m-\nu,\ m+1,\ A/(A+B));\quad(35)$$

$$J^{(\nu)}_{M=2m+1}=0;\quad G_0(x\varepsilon)=\frac{qxg(x\varepsilon)}{\sqrt{A(x\varepsilon)[A(x\varepsilon)+B(x\varepsilon)]}}.\quad(36)$$

Here $F(a, b, c, d)$ is a hypergeometric function. In practice it suffices to confine oneself in (35) to second-order $1/(qx)^2$, and for $L\neq0$ the main contribution to (34) is made by the terms with $M=0$. In Appendix 2 are given the derivation of (35) and the expressions for G_{LM} at $L=2$ and 3.

Thus, the subsequent task of finding the form factor reduces to a calculation of the one-dimensional integrals (33). This can be done numerically by choosing a suitable upper integration limit, since the explicit forms of the integrands are obtained only for the region of the principal contribution in the vicinity $x\lesssim R$ of the nucleus. The answer can, however, be obtained also in explicit form by using the properties of the expressions $\rho_L(x)$, which are typical for many calculations. We present below two such examples.

Pole Method of Calculating the Elastic-Scattering Form Factor for a Fermi Density

In the analysis of elastic scattering of electrons by medium and heavy nuclei one uses most frequently a Fermi charge-density distribution

$$\rho_F(x)=\rho_0(x)\,Y_{00}(\hat{x})=\rho^{(0)}\cdot\frac{1}{1+\exp[(x-R)/b]},\quad(37)$$

where $\rho^{(0)}$ is defined by the normalization condition

$$\int\rho_F(x)\,dx=1;\quad(38)$$

R is the density half-value parameter; b is the thickness of the surface of the nucleus. The form factor (33) now becomes

$$F^F(q,E)=F^F_{00}(q,E)=2\pi iq\rho^{(0)}\sum_{\varepsilon=\pm1}\varepsilon\int_0^\infty\frac{G_0(x\varepsilon)}{q^2_{\text{eff}}(x\varepsilon)}$$
$$\times\exp\{i[qx\varepsilon+\phi(x\varepsilon)]\}\frac{x\,dx}{1+\exp[(x-R)/b]}.\quad(39)$$

To calculate the radial integral, we use the fact that the function (37) has simple poles at the complex-plane points[8]

$$x^\varepsilon_s=R+i\pi b\varepsilon(2s+1),\quad s=0,\ 1,\ 2,\ \ldots;\ \varepsilon=\pm1.\quad(40)$$

We first analyze the simplest case of the Born approximation ($\phi=0$, $G_0=1$, $q_{\text{eff}}=q$). Then

$$F^F(q)=\frac{2\pi i}{q}\rho^{(0)}\sum_{\varepsilon=\pm1}\varepsilon\int_0^\infty W(x\varepsilon)\,dx;\quad(41)$$

$$W(x\varepsilon)=\frac{\exp(iqx)\,x}{1+\exp[(x-R)/b]}.\quad(42)$$

Representing the integrals (41) in the form

$$\sum_{\varepsilon}\varepsilon\int_0^\infty W(x\varepsilon)\,dx=\sum_{\varepsilon}\varepsilon\left\{\oint-\int_{C(\varepsilon)}-\int_{i\varepsilon\infty}^{0}\right\}W(x\varepsilon)\,dx,\quad(43)$$

where the circling directions are shown in Fig. 1, we see that the integrand has poles at the points (40) and tends to zero on circles $C^{(\varepsilon)}$ of infinite radius in the first quad-

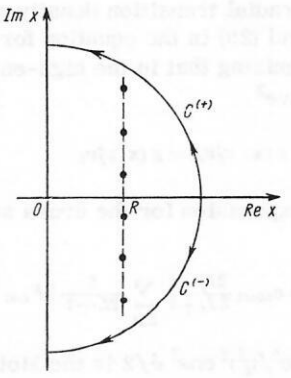

Fig. 1. Choice of integration contours.

rant (where $\varepsilon = -1$). The contribution from the imaginary axis is conveniently estimated directly for the difference

$$\Delta| = \Big| \sum_{\varepsilon} \varepsilon \int_{i\varepsilon\infty}^{0} W(x\varepsilon)\, dx \Big| = \Big| \sum_{\varepsilon} \varepsilon \int_{0}^{\infty} \frac{\exp(iq\rho)\,\rho\, d\rho}{1+\exp(-R/b)\exp(i\varepsilon\rho/b)} \Big| < \Big| \frac{-2i\exp(-R/b)\sin[2\operatorname{arctg}(1/qb)]}{(1-\exp(-R/b))^2(q^2+1/b^2)} \Big| . \quad (44)$$

It will be shown below that this contribution can be neglected because $\exp(-R/b)$ is small. In addition, as $q \to 0$ we have $|\Delta| \to 0$. Thus, the form factor is determined by the residues at the poles (40) and can be expressed in the form

$$F^F(q) = -\frac{8\pi^2}{q}\rho^{(0)}Rb\sum_{s=0}^{\infty}\Big(\cos qR - (2s+1)\frac{\pi b}{R}\sin qR\Big) \times \exp[-(2s+1)\pi bq]. \quad (45)$$

At sufficiently large $q > 1$, the main contribution to (45) is made by the first term of the series with $s = 0$, since each succeeding term is smaller than the preceding term by a factor $\exp(2\pi bq)$ and can be neglected if $2\pi bq \gg 1$. In (45), however, it is possible to carry out exact summation by using

$$\sum_{s=0}^{\infty}\exp[-(2s+1)x] = \frac{1}{2\operatorname{sh} x}; \quad \sum_{s=0}^{\infty}(2s+1)\exp[-(2s+1)x] = \frac{\operatorname{cth} x}{2\operatorname{sh} x}. \quad (46)$$

As the result we obtain for the Born form factor for elastic scattering of electrons by a nucleus with a Fermi density the final expression[8]

$$F^F(q) = -\frac{8\pi^2}{q}\rho^{(0)}Rb\Big[\cos qR - \frac{\pi b}{R}\sin qR\operatorname{cth}\pi bq\Big]\frac{1}{2\operatorname{sh}\pi qb}. \quad (47)$$

From this follows in the limiting case $b \to 0$ an expression for the form factor of a step-function charge-density distribution:

$$F^0(q) = \lim_{b\to 0} F^F(q) = \frac{3}{(qR)^2}\Big(\frac{\sin qR}{qR} - \cos qR\Big). \quad (48)$$

Expression (47) can be used to analyze qualitatively the cross sections for scattering of electrons by medium and heavy nuclei. We shall show below that for light nuclei this expression can be used also for quantitative comparisons. Comparing (47) with the estimate (44), we obtain an upper bound on the region of its applicability:

$$q < R/(\pi b^2), \quad (49)$$

which yields a value close to the contemporary experimental limit of cross-section measurements.

We now consider the same problem of scattering by a nucleus with a Fermi density (37), but with allowance for the distortion of the wave function of the electron in the Coulomb field of the nucleus. We use the same pole method. It is now necessary to take into account also the poles due to the functions $G_0(x\varepsilon)$ and $q^2_{\text{eff}}(x\varepsilon)$. Analysis shows that they lie far from the poles x_s^{ε} [Eq. (40)] and that their contribution is negligibly small. Further, the presence of the function $\phi(x\varepsilon)$ in the argument of the exponential changes the behavior of the integrand on the contour $C^{(\varepsilon)}$. It must be remembered here, however, that at large $|x|$ it is necessary to use for it the exact asymptotic value $\phi \to 2Ze^2 \cdot \ln 2kx$, and not the value obtained above, which is valid only in the vicinity of the nucleus. At the true value of ϕ, the integral along the contour $C^{(\varepsilon)}$ turns out to tend to zero. The difference between the integrals on the imaginary axis is also bounded from above by the estimate (44). Thus, the integral (39) is again determined by the poles of the Fermi density, and is equal to

$$F^F(q,E) = -4\pi^2 q\rho^{(0)}b\sum_{s=0}^{\infty}\sum_{\varepsilon=\pm 1} \times\Big\{\frac{G_0(x_s^{\varepsilon}\varepsilon)}{q^2_{\text{eff}}(x_s^{\varepsilon}\varepsilon)}x_s^{\varepsilon}\exp\{i[\varepsilon qx_s^{\varepsilon} + \phi(x_s^{\varepsilon}\varepsilon)]\}\Big\}. \quad (50)$$

At $R \gg b$ and $q > 1$, this series converges rapidly because of the factor $\exp(-\pi bq(2s+1))$, so that in practice we can confine ourselves to the zero-order term with $s = 0$. However, it is possible here, too, to sum over s, taking outside the summation sign the weak function $(G_0/q^2_{\text{eff}})\exp(i\phi)$ at the point x_0^{ε} of the principal contribution. We then obtain the following final result for the form factor of elastic scattering by a nucleus with the Fermi density:

$$F^F(q,E) = -4\pi^2 q\rho^{(0)}b\sum_{\varepsilon=\pm 1}\frac{G_0(x_0^{\varepsilon}\varepsilon)}{q^2_{\text{eff}}(x_0^{\varepsilon}\varepsilon)} \times (R + i\varepsilon\pi b\operatorname{cth}\pi bq)\frac{\exp\{i[\varepsilon qR + \phi(x_0^{\varepsilon}\varepsilon)]\}}{2\operatorname{sh}\pi bq}. \quad (51)$$

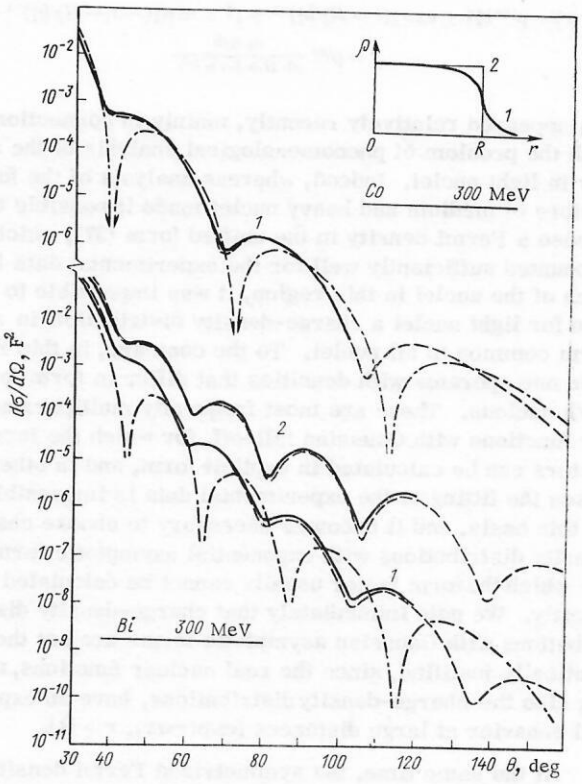

Fig. 2. Comparison of the methods of calculating the electron elastic-scattering cross section: solid lines) phase-shift analysis, dashed lines) high-energy approximation, dash–dot lines) Born approximation (taken from ref. 8).

In the limit as $b \to 0$, this yields an expression previously obtained in ref. 7 for the form factor with a step-function charge-density distribution.

Expression (51) can be used for direct calculations and for comparison with experiments on electron scattering by medium and heavy nuclei, if the conditions of the high-energy approximation $kR \gg Z/(137kR) \ll 1$ are satisfied in the angle region $\vartheta > \vartheta_0 \sim 1/kR$; $q < q_0 < R/\pi b^2$. Thus, Fig. 2 shows a methodological comparison[8] of the cross sections for elastic scattering of electrons by the nuclei (R = 4.19 F, b = 0.52 F) and Bi (R = 6.64 F, b = 0.56 F) at an electron energy E = 300 MeV ($k = 1.5204$ F^{-1}), calculated by the phase-shift-analysis method,[10] by the high-energy-approximation method and relation (51) and in the Born approximation (47). We see that there is good agreement between the phase-shift-analysis and high-energy-approximation calculations. The slight discrepancy at large angles in the case of bismuth is due to the use of approximate functions and an approximate method of calculating the angle integral in the high-energy approximation.

Thus, the high-energy-approximation expressions obtained describe well the cross sections for scattering by medium and heavy nuclei, and they can be conveniently used for a quantitative analysis of the experimental data, owing to the explicit dependence on the density parameters R and b and on the electron energy E.

Form Factor for Symmetrized Fermi Density

Interest in the use of the symmetrized Fermi density

$$\rho_{SF}(r) = \rho^{(0)}[\{1+\exp[(r-R)/b]\}^{-1} + \{1+\exp[(-r-R)/b]\}^{-1} - 1] = \rho^{(0)} \frac{\operatorname{sh} R/b}{\operatorname{ch} R/b + \operatorname{ch} r/b} \quad (52)$$

has appeared relatively recently, mainly in connection with the problem of phenomenological analysis of the decay in light nuclei. Indeed, whereas analysis of the form factors of medium and heavy nuclei made it possible to choose a Fermi density in the unified form (37), which accounted sufficiently well for the experimental data for each of the nuclei in this region, it was impossible to obtain for light nuclei a charge-density distribution in a form common to all nuclei. To the contrary, in this region one operates with densities that differ in form for each nucleus. These are most frequently multiparameter functions with Gaussian fall-off, for which the form factors can be calculated in explicit form, and in other cases the fitting to the experimental data is impossible on this basis, and it becomes necessary to choose charge-density distributions with exponential asymptotic form, for which the form factor usually cannot be calculated explicitly. We note immediately that charge-density distributions with Gaussian asymptotic forms are not theoretically justified, since the real nuclear functions, meaning also the charge-density distributions, have an exponential behavior at large distances [$\exp(-\alpha r)$, $r > R$].

At the same time, the symmetrized Fermi density has the following important features. First, it is a simple two-parameter function, where R determines the density half-value and b determines the width of the charge-density-distribution surface layer. Second, it decreases at large r in accordance with a correct exponential law. Third, at the center of the nucleus this density always flattens out, thereby differing from the Fermi density (37), which has a nonzero derivative at r = 0. To be sure, for medium and heavy nuclei, where this function is used, the latter circumstance is immaterial, inasmuch as $\rho'_F(0) \ll 1$ and both densities practically coincide. For light nuclei, on the other hand, this derivative is not small, and here the density (52) offers the same advantages as a Gaussian density.

Finally, the form factor corresponding to the density (52) can be calculated in analytic form.[11] It is also possible, in an equally explicit form, to find the density normalization constant $\rho^{(0)}$ and the rms radius:

$$\rho^{(0)} = \frac{3}{4\pi R^3}[1 + (\pi b/R)^2]^{-1}; \quad (53)$$

$$\overline{R} = \langle r^2 \rangle^{1/2} = R\sqrt{\frac{3}{5}}\sqrt{1 + \frac{7}{3}\left(\frac{\pi b}{R}\right)^2}. \quad (54)$$

All this is very valuable for the practical reduction of the experimental data and when the form factor is used in other theoretical investigations.

To obtain an explicit expression for the Born form factor with a symmetrized Fermi density

$$F_B^{SF}(q) = \frac{4\pi}{q}\int_0^\infty \sin(qr)\rho_{SF}(r)\,r\,dr, \quad (55)$$

we use the known integral[12]

$$J(q) = \int_0^\infty \frac{\cos qr\,dr}{\operatorname{ch} R/b + \operatorname{ch} r/b} = \frac{\pi b}{\operatorname{sh} R/b}\cdot\frac{\sin qR}{\operatorname{sh} \pi b q}. \quad (56)$$

Then, substituting (52) in (55), we find

$$F_B^{SF}(q) = -\frac{4\pi}{q}\rho^{(0)} \operatorname{sh} R/b \cdot \frac{d}{dq} J(q) \quad (57)$$

or

$$F_B^{SF}(q) = -\frac{4\pi^2 b R \rho^{(0)}}{q \operatorname{sh} \pi b q}(\cos qR - (\pi b/R)\sin qR \operatorname{cth} \pi b q). \quad (58)$$

It is interesting that the exact expression for the Born form factor with ρ_{SF} coincides with the approximation (47) for the Fermi density ρ_F obtained by the pole method, neglecting the contribution from the imaginary axis. It is now clear that the appearance of this nonvanishing contribution is due to the poor analytic properties of the Fermi function, namely to the fact that its derivative differs from zero at the point r = 0.

We note also some features of this form factor. Foremost among them is exponential decrease with increasing q:

$$F(q) \sim \exp(-\pi b q), \quad (59)$$

which conforms with the experimental behavior at $q > 1$. It is seen that this fall-off is steeper, the larger the smearing of the charge in the surface layer of the nucleus. Further, the form factor (58) has theoretical zeros at the points q_s defined by the equation

$$\operatorname{tg} q_s R = (R/\pi b) \operatorname{th} \pi b q_s, \quad (60)$$

this being a consequence of the finite dimensions of the nucleus. In experiment, these points correspond to minima of the differential cross sections.

It will be necessary later on to compare the results of the Born calculation with calculation by the high-energy approximation. Without presenting the details of the calculations of the form factor within the framework of the high-energy approximation, we indicate only that the procedure itself is similar to that described above. The explicit form of the form factor is obtained again after replacing an integral of the type (41) by two integrals along contours of infinite radius in the first and fourth quadrants and summing the resultant residues at the poles of the function (52) $r_s = R \pm i\pi b(2s+1)$, $s = 0, 1, 2, \ldots$. The results can be represented in the form

$$F^{SF}(q, E) = -\frac{4\pi^2 bR\rho^{(0)}}{q \operatorname{sh} \pi bq} D[\cos(qR+\Phi) - (\pi b/q)\sin(qR+\Phi)\operatorname{cth}\pi bq], \quad (61)$$

where D and Φ are complex functions of q and E and take into account the distortion. They can easily be determined by comparison with the analogous equation for the Fermi form factor (51). Naturally, in the Born approximation we obtain $D = 1$ and $\Phi = 0$.

2. ELASTIC SCATTERING

The investigation of elastic scattering (mainly of the charge form factors) includes the determination of the detailed behavior of the charge-density distribution for each individual nucleus, and also the behavior of the "average" nuclear characteristics (radius, diffuseness, etc.) with changing atomic number and changing nuclear structure. The solution of this problem is hindered by the incomplete development of such methods for the analysis of experimental form factors as the determination of the inverse Fourier transforms of integrals with finite upper limits or the corresponding mathematical methods optimizing incorrectly formulated problems. It is precisely these methods which can yield model-independent information on the charge-density distribution function of the nucleus, which can then be compared with the predictions of the nuclear models. The difficulties of such an analysis (which are frequently fundamental in nature) make it necessary to resort to a simpler direct or model-dependent method, wherein one first obtains the charge-density distribution within the framework of a definite calculation scheme or nuclear model, and the subsequently calculated form factors are compared with the experimental ones. As to the "average" characteristics of the nucleus, the most economical in this case is an analysis based on phenomenological charge-density distributions chosen on the basis of very simple physical considerations regarding the structure of the ground states of the nuclei. This reveals more or less reliably certain parameter-behavior features that are common to a group of nuclei, depending, e.g., on the character of the filling of the shells, of the isotopic shifts, of the "softness of the nucleus" relative to collective excitations, etc. We shall discuss some of these questions in detail.

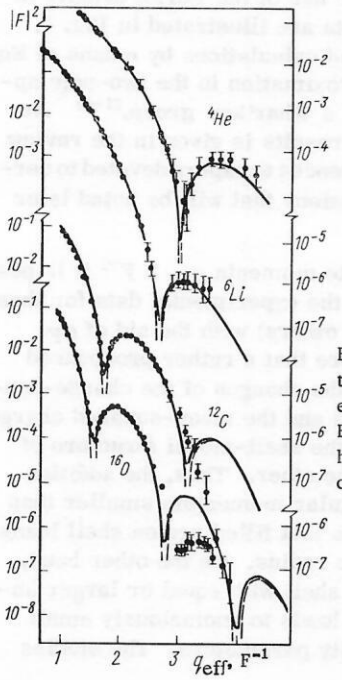

Fig. 3. Form factors for elastic scattering by light nuclei in the high-energy approximation for a symmetrized Fermi density: solid curves) exact high-energy approximation; dashed curves) Born approximation.[11]

Analysis of Form Factors with the Aid of Phenomenological Charge-Density Distributions

The method consists of choosing a definite form of the charge-density distribution and calculating the corresponding form factors. Each nucleus has its own individual structure. Therefore an analysis on the basis of a single form of the charge-density distribution is meaningful only for a group of nuclei. Its purpose is to find the principal regularities in the behavior of the general characteristics of nuclei, such as the mean-squared radii, isotopic and isotonic shifts of the parameters, deviations of the course of the form factors of concrete nuclei from their general behavior, etc. It is possible sometimes to describe in this case quite accurately also the entire form factor of some individual nucleus; this does not mean, however, that the "experimental" charge-density distribution of the given nucleus has been obtained in this way. The possible errors of such an interpretation will be discussed later on.

The choice of the charge-density distribution function is usually based on general properties of the nucleus, such as its incompressibility, the behavior of the single-particle functions near and outside the nuclear surface, etc. It becomes necessary to take into account also the traditions that have developed over twenty years. We shall dwell on the main problems and results of the application of this approach to analysis of the experimental data.

Light nuclei. Earlier, when experimental data were available for only small momentum transfers q, it turned out to be sufficient for their description to choose a simple Gaussian charge-density distribution function $\exp(-r^2/a^2)$ and multiply by a factor $(1 + b^2r^2)$, and this imitated the "bump" of the density in the region of the nuclear surface. The Born form factors for these charge-density distributions can be calculated in explicit form, thereby definitely adding to the convenience in the analysis of the experiment. With appearance of new data at large q, the desire to describe the entire form factor has led to a complication of these simple charge-density distribution functions. Multiparameter Gaussian densities

appeared for each individual nucleus (see, e.g., refs. 13-15). Their shortcomings are obvious, namely the resultant nonrealistic Gaussian asymptotic form and the large number of parameters (sometimes 5 to 8). We emphasized earlier the advantage of a density of a different type, namely the symmetrized Fermi function

$$\rho_{SF}(r) = \rho^{(0)} \frac{\operatorname{sh} R/b}{\operatorname{ch} R/b + \operatorname{ch} r/b}, \qquad (62)$$

which leads to explicit expressions for the Born and high-energy form factors. To demonstrate the advantages of this density in the phenomenological analysis of light nuclei, let us examine the results of form-factor calculations made for this function,[11] shown in Fig. 3 and plotted as functions of the effective momentum transfer

$$q_{\text{eff}} = q\left(1 + \frac{4}{3}\cdot\frac{Z}{137}\cdot\frac{1}{\overline{R}(A)\cdot E}\right), \qquad (63)$$

in which account is taken of the dependence of the experimental form factors on the energy. It is seen that the charge-density distribution (62) leads to full agreement with experiment for the nuclei ^{4}He and ^{6}Li. Only at the largest measured values of $q \geqslant q_0$ (4.4 and 3.5 F^{-1} for ^{4}He and ^{6}Li, respectively) do the calculated curves exhibit a tendency to deviate from the experimental one. We conclude therefore that the introduction of a large number of parameters to the Gaussian charge-density distribution for these nuclei was needed primarily to correct the character of its fall-off in the surface layer of the nucleus and to make it exponential. Thus, the region $q < q_0$ can be called the region of "small" momentum transfers, where the behavior of the form factor is determined mainly by the distribution of the charge density on the nuclear boundary.

For the nuclei ^{12}C and ^{16}O, the density (62) describes well the experimental data up to $q_0 \approx 3.2$ F^{-1} (^{12}C) and $q_0 \approx 2.85$ F^{-1} (^{16}O), while at $q > q_0$ the theoretical calculations begin to deviate patently from the experimental values of the form factors. This means that at large $q > q_0$ the behavior of the form factors depends on the character of the density distribution in the central region of the nucleus, so that to improve the agreement with experiment in this region it is necessary to take into account the peculiarities of the behavior of the charge-density distribution within the nucleus.

It appears that the first deviations of this type were pointed out in the analysis of the experiments on the medium nuclei ^{40}Ca and ^{48}Ca (ref. 16). The same can be stated now concerning the light nuclei. Moreover, these deviations could be noted here even before the experiments were performed on the Ca isotopes, but their observation was hindered by the traditional analysis method, wherein a specialized form of the charge-density distribution was chosen for each nucleus. An impression was gained that the specifics of the structure of light nuclei becomes manifest starting even with small q, and that rather than seek the "deviations" it is necessary to perform direct calculations of the charge-density distribution within the framework of nuclear models with allowance for all the peculiarities of each nucleus.

The values of the mean-squared radii $\overline{R}$ and of q_0 obtained as a result of χ^2 calculations at $q < q_0$ for each of the nuclei considered showed that even though $\overline{R}$ and q_0 are different for each of the nuclei, their product remains constant with an error of 10%, $q_0\overline{R} = 8.5(\pm 10\%)$.

The scatter here is due both to the appearance of a structure that is to a certain degree individual for each of the nuclei, especially ^{6}Li, which exhibits a "loose" surface structure, and to the weak tendency of this quantity to grow with increasing atomic number (of the nucleus). In other words, for all the nuclei the form factors "begin to feel" the deviations of the real charge-density distributions from the homogeneous "flattop" behavior in the internal region, starting only with a definite value of the momentum transfer $q > q_0 = 8.5\overline{R}^{-1}$ F^{-1}, which is rigorously connected with the dimensions of the nucleus. At $q < q_0$, the behavior of the form factor is determined mainly by the structure of the charge-density distribution in the region of the surface.

Figure 3 leads also to a general conclusion that the Born calculations can be used for light nuclei. It is seen that their deviations from the exact ones become noticeable only when q and Z are increased, so that starting with ^{16}O the Born approximation can be used more readily for qualitative than for quantitative comparisons.

Medium and heavy nuclei. It is traditional here to use the phenomenological Fermi density

$$\rho_F(r) = \rho^{(0)} \frac{1}{1 + \exp[(r-R)/b]}, \qquad (64)$$

even though, as already noted, this density practically coincides for these nuclei ($R \gg b$) with the symmetrized Fermi density (62). Nonetheless, many calculations were performed with a charge-density distribution in the form (64), and led to certain general conclusions concerning the structure of the ground states of such nuclei. Naturally, the Born approximation no longer holds here and allowance for the distortions is obligatory.

Typical examples of the use of the Fermi density in analysis of experimental data are illustrated in Fig. 4. which shows certain data and calculations by means of Eq. (50) of the high-energy approximation in the two-pole approximation, performed by a Khar'kov group.[21-23] An analysis of these and other results is given in the review 24, which contains also references to papers devoted to certain questions and to conclusions that will be noted later on.

It is seen first that up to momenta $q \sim 2$ F^{-1} it is possible to obtain a good fit to the experimental data for these nuclei (and for a number of others) with the aid of ρ_F. The authors note furthermore that a rather pronounced correlation exists between the changes of the charge-density distribution parameters and the mean-squared charge radii, on the one hand, and the shell-model structure of the investigated nuclei on the other. Thus, the addition of neutrons with orbital angular momentum smaller than the orbital momentum of the last filled proton shell leads to an increase in the charge radius. On the other hand, if the neutron is added to a shell with equal or larger angular momentum, then this leads to anomalously small changes in the proton-density parameters. The studies

of isotopic effects of this type, using Ca and Ti isotopes, were started quite some time ago.[18-20] To interpret the isotopic deviations obtained in this manner it is necessary frequently to resort to modern microscopic models of the nucleus.

Another, but as yet less definite, conclusion concerns the comparison of a large number of data on the scattering of electrons and protons by nuclei. A reduction of these data shows that, with aceptable accuracy, the charge radii are characterized by the relation

$$\langle r^2\rangle_Z^{1/2} \sim (2Z)^{1/3}, \tag{65}$$

whereas for the nuclear-matter distribution (data on the scattering of protons and α particles) the rms radius is

$$\langle r^2\rangle_A^{1/2} \sim A^{1/3}. \tag{66}$$

Comparing these results, we can advance the hypothesis that the nuclei possess a "neutron jacket," whose thickness amounts to approximately 0.5 F.

It is interesting that a similar conclusion is arrived at in a study[25] of the scattering of protons of high energy by nuclei, where the data were reduced by the multiple-scattering method[3] using a Fermi distribution of nuclear matter in the form (64), and these data were compared with the already known charge-density distributions.

It has already been noted that to describe the form factors in the region of large q it is necessary to introduce new parameters in the phenomenological charge-density distributions. One of the successful forms in this case was a Fermi-like function of the type

$$\rho = \rho^{(0)}(1 + wr^2/c^2)\{1 + \exp[(r^n - c^n)/t^n]\}^{-1}. \tag{67}$$

At n = 1 this density is close to (64), and we shall therefore not discuss studies in which this function was used as a fit test, and consider only the case n = 2.

Figures 5 and 6 show some results of comparison with experiment,[26,27] where an optimal fit yielded a value n = 2, i.e., a Fermi-like function with Gaussian asymptotic form was arrived at. Arguments favoring this type of charge-density distribution can be advanced with the aid of a simple single-particle model, where the charge-density distribution is constructed as the sum of the squares of the moduli of the functions of the bound states of protons from all the nuclear shells in the ground state, $\rho(r) = \sum_n |\psi_n(r)|^2$. Naturally, at $r \gg R$ the asymptotic density is determined by only one function, having a slight exponential fall-off, of the upper shell. At $r \approx R$ the functions of all shells make approximately equal contributions, but these functions have different exponential decreases. It appears that the plot of the total contribution can be parametrized by a Gaussian curve in a certain region of the nuclear periphery $\rho(r \gtrsim R) \approx \sum_n a_n \exp(-2\sqrt{2E_n m/\hbar^2}\, r)$. At the same time it is probable that it is this region which makes the largest contribution to the form factor at large q.

A similar feature of the charge-density distribution should be manifest more strongly in relatively heavy nuclei, where many shells take part in the formation of the density, and less strongly in light nuclei. This hypothesis is confirmed to some degree by Fig. 5. We note, finally, that excessive confidence in the interpretation of the form factor of an individual nucleus with the aid of phenomenological densities can lead to erroneous results. A typical example is the phenomenological analysis of the ^{208}Pb nucleus.[27] It is seen from Fig. 6 that the obtained best-fit density (67) has at n = 2 a dip at the center of the nucleus. On the other hand, many calculations by the Hartree–Fock method and in a single-particle model with a Woods–Saxon potential[27] yield a stable rise of the charge-density distribution at this location. We shall show below that the reason for this disparity is the ambiguity of the use of such an

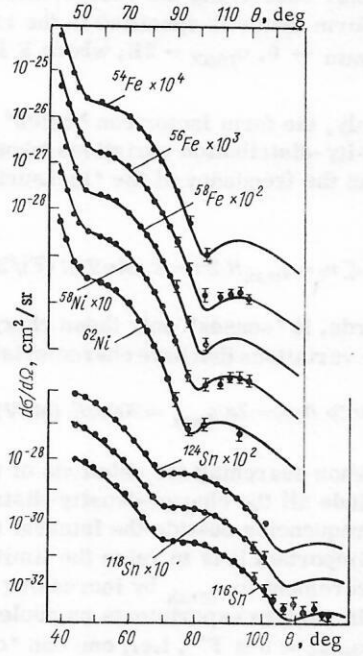

Fig. 4. Analysis based on the Fermi density of isotopic effects in elastic scattering of electrons.[21-23]

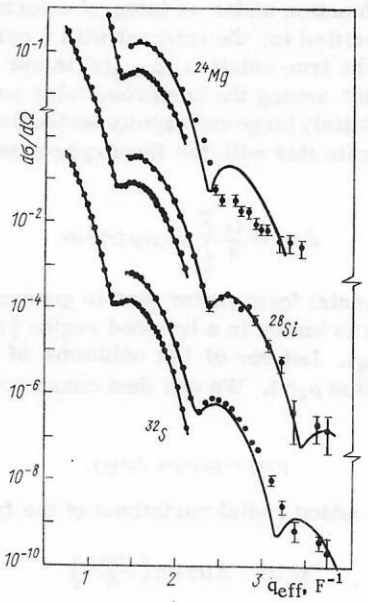

Fig. 5. Fit of a parabolic Fermi-like density with Gaussian asymptotic form to the experimental data.[26]

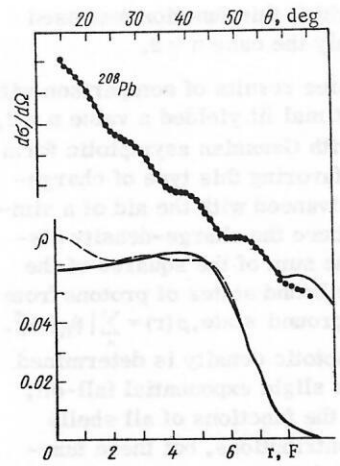

Fig. 6. Form factor of the ^{208}Pb nucleus, calculated with the aid of a parabolic Fermi-like density; dashed curve) calculation of the charge-density distribution by the independent-particle model on the basis of the Woods–Saxon potential.[27]

analysis of the experimental data to search for an "experimental" charge-density distribution of a concrete nucleus. It turns out that there exist also other charge-density distributions that describe equally well the same experiment but conform to the theoretical predictions.

Model-Independent Analysis

To understand the successes and failures of the phenomenological approach to the description of form factors of particular nuclei, we must return to certain general questions, namely: What information on the charge-density distribution can be extracted from a specified experimental form factor? How can we formulate mathematically the problem of its model-independent analysis? What kind of additional information and limitations must be introduced in this analysis?

We note immediately that within the framework of a purely mathematical formulation of the problem it is impossible to determine the charge-density distribution function directly from the experimental form factor, which is always "inaccurate." The point is that this is an incorrectly formulated problem, in which it is required to determine the function under an integral-operator sign from the value specified for the integral with a certain error. In this case the true solution [$\rho_{exp}(r)$ in our case] is always "mislaid" among the numerous false solutions that contain indefinitely large and rapidly oscillating components. Let us illustrate this with the Born approximation as an example:

$$F(q)=\frac{4\pi}{q}\int_0^\infty \sin qr\rho(r)\,r\,dr. \tag{68}$$

The experimental form factor (and in general only its absolute value) is known in a bounded region $\{q_i\}$ with an error $\pm\Delta F(q_i)$. Let one of the solutions of (68) be the smooth function $\rho_0(r)$. We can then construct another solution

$$\rho(r)=\rho_0(r)+\Delta\rho(r), \tag{69}$$

to which are added radial variations of the type

$$\Delta\rho(r)=A(r)\sin\left(\frac{2\pi nr}{R}\right) \tag{70}$$

with amplitude A(r) and with rapid oscillations (n is large) within the limits of the nuclear radius R. For any A(r) we

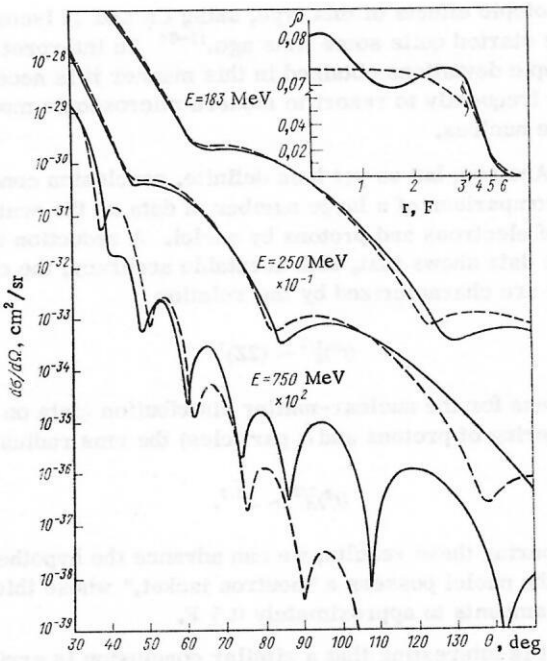

Fig. 7. Energy dependence of the differential cross sections for electron scattering[9] by ^{58}Ni for a Fermi density (dashes) and for the density from ref. 28 (solid curves).

can find a value of n such that the form-factor increments resulting from the substitution of (69) in (68) remain within the limits of the form-factor errors. Strictly speaking, the true solution of (68) is obtained by taking the inverse Fourier transform of the exact function F(q), but since such a function cannot be obtained by experiment, it is meaningless to formulate the problem in this manner.

Thus, the problem reduces to finding a way of separating the physically admissible solutions from all the possible solutions when $\rho(r)$ is to be determined from (68). We first assess the information that can be extracted from the form factor concerning the charge-density distribution, if the form factor is specified in the range $q_{min} < q < q_{max}$ ($q_{min} \to 0$, $q_{max} \to 2E$, where E is the electron energy).

Obviously, the form factor can "catch" only those charge-density-distribution variations whose frequency is lower than the frequency of the "measuring" function, i.e.,

$$n \ll n_0 = q_{max}R/2\pi = E\,(\text{MeV})R\,(\text{F})/200\pi, \tag{71}$$

in other words, it "senses" only those charge-density-distribution variations that have characteristic wavelengths:

$$\Delta r \gg R/n_0 = 2\pi/q_{max} = 200\pi/E\ (\text{MeV}),\ \text{F}. \tag{72}$$

Thus, when searching for solutions of (68) it is necessary to exclude all the charge-density-distribution variations with frequencies outside the interval (71). This also shows how important it is to raise the limit of the form-factor measurement to q_{max} by increasing the electron energy E. In modern experiments on nuclei, the limiting values are $q_{max} \approx 3$–$4\ \text{F}^{-1}$, i.e., one can "catch" physical variations of the charge-density distribution in an interval $\Delta r \simeq 1.5$–2 F. Figure 7 shows[9] the variation of the "sen-

sitivity" of the form factor to details of the charge-density distribution with increasing electron energy. It is seen that even a fairly smooth variation of the charge-density distribution becomes manifest in the scattering-angle region that lends itself to measurements only at a sufficiently high energy E ≃ 500 MeV and higher.

We note now the most general features of the charge-density distribution, which must be taken into account when physical solutions of (68) are sought:

1) exponential fall-off at r ≫ R;

2) the appearance of a "bump" in the region of the nuclear surface at r ~R, which is a consequence of the "flex" of the single-particle functions on going from an exponential decrease outside the nucleus to saturation or oscillations in the interior;

3) The number of possible radial variations $\Delta\rho(r)$ of the charge-density distribution should be determined, roughly speaking, by the number of nuclear shells;

4) the minimum dimension of the variation should not exceed the dimension of the nucleon ($\Delta r > 1$ F).

All these features are quite successfully accounted for in the basis of charge-density-distribution trial functions made up of derivatives of the Fermi density.[9] First, the zeroth harmonic $\rho_0 = \rho_F(r)$ guarantees agreements with experiment at low and medium q owing to its exponential fall-off. Second, $\rho'_F(r)$ gives a "bump" at r ~R. Finally, the remaining derivatives $\rho_F^{(n)}(r)$ make it possible to describe any spectrum of the radial variations of the charge-distribution density outside the nucleus, since it is possible to make up from them a complete set of functions:

$$\{\phi_n\} = \{\sum_k \alpha_k^n \rho_F^{(k)}(r)\}. \tag{73}$$

One more advantage of this set is that explicit expressions for the form factors are available within the framework of the high-energy approximation for all the derivatives $\rho_F^{(n)}(r)$. Thus, a charge-density distribution of any type can be represented in the form[9]

$$\rho(r) = \sum_{n=0}^{N} a_n \rho_F^{(n)}(r) = \sum_{n=0}^{N} C_n \frac{\partial^n}{\partial R^n} \rho_F(r, R). \tag{74}$$

Substituting this expression in the form factor (23), we obtain

$$F = \sum_n C_n F_F^{(n)}, \tag{75}$$

where

$$F_F^{(n)} = \frac{\partial^n}{\partial R^n} F_F. \tag{76}$$

Inasmuch as the form factor F_F of the Fermi density is known in its explicit form (39), we can, by calculating its derivatives, obtain[9]

$$F^{(n)}(q, E) = -4\pi^2 q b^2 \rho_0^{(0)} (-i)^{n-1} \sum_{\varepsilon=\pm 1} \frac{G(x_0^\varepsilon, \varepsilon)}{q_{\text{eff}}^2(x_0^\varepsilon, \varepsilon)}$$
$$\times [b q_{\text{eff}}(x_0^\varepsilon, \varepsilon)]^{n-1} [n + i q_{\text{eff}}(x_0^\varepsilon, \varepsilon) R - \varepsilon q_{\text{eff}}(x_0^\varepsilon, \varepsilon) \pi b \operatorname{cth} \pi q b]$$
$$\times \frac{\exp i[\varepsilon q R + \phi(x_0^\varepsilon, \varepsilon)]}{\operatorname{sh} q\pi b}. \tag{77}$$

At n = 0 this expression goes over into the ordinary Fermi-density form factor (39).

To realize technically such a program of selecting only the physically reasonable charge-density distributions corresponding to the conditions formulated above, one can in principle use the Tikhonov method of regularizing the solution,[29] wherein one minimizes the functional

$$\sum_i |F_{\text{theor}}(q_i) - F_{\text{exp}}(q_i)|^2 + \alpha \int \left(\frac{\partial \rho(r)}{\partial r}\right)^2 dr, \tag{78}$$

where, unlike the usual χ^2 method, there is an additional term that excludes the contribution of the rapidly oscillating components to the integrand function $\rho(r)$ of (68). This contribution can be regularized by selecting the parameter α. In practice, however, it is simpler just to specify the error corridors of the amplitudes A(r) and of the frequencies of n trial functions of the type (69). Then, by fitting the form factor (75) to the experimental data and determining the corresponding parameters R and b and the coefficients $\{C_n\}$, we can use them to "reconstruct" the model function which is independent of the charge-density distribution on the basis of (74).

Such a program for a model-independent analysis was first proposed and realized, with electron scattering by ^{40}Ca and ^{48}Ca as an example, in refs. 9 and 30. We present below several examples from ref. 30.

The method described was used for a model-independent analysis of elastic scattering of electrons by ^{40}Ca (E = 250 and 750 MeV) and ^{48}Ca (E = 750 MeV).

The availability of data for ^{40}Ca at 250 MeV (ref. 31, data I) and 750 MeV (ref. 32, data II) makes it possible to trace the manner in which the uncertainty of the obtained charge-density distributions becomes narrower with increasing measured region of the momentum transfers from $q_{max} = 2$ to $q_{max} = 3.3$ F^{-1}.

Figure 8 shows certain typical results of the model-independent analysis of data I for ^{40}Ca. It is seen that the agreement with experiment for all the charge-density distributions is almost complete, but in the region $\vartheta > 125°$,

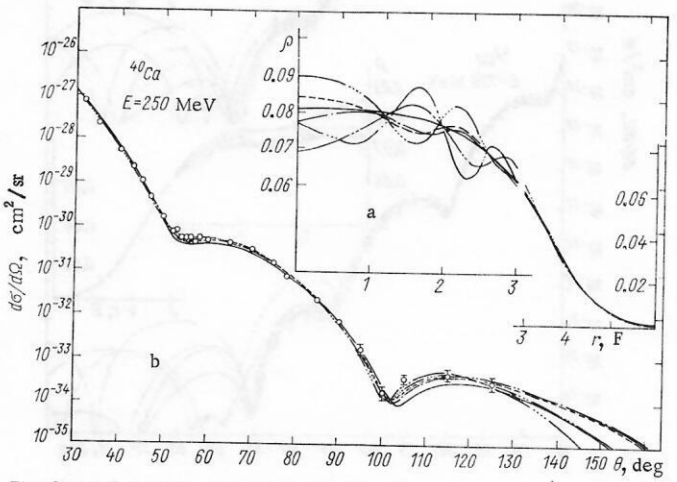

Fig. 8. Model-independent analysis of the data on the elastic scattering of 250-MeV electrons by ^{40}Ca: a) charge-density distributions; b) the corresponding cross sections, ——) Fermi density, – –, –·–, –··–, –····–, ——) obtained from a model-independent analysis.[30]

where the cross section was not measured, the curves differ noticeably from one another. We can thus conclude that by using the data at E = 250 MeV (small q) we can determine the charge-density distributions with the aid of the model-independent analysis only in the region of the surface fall-off. On the other hand, inclusion of the density variations in the central region of the nucleus, with amplitudes on the order of ±20% of the mean value of the charge-density distribution, and with a frequency of two or three variations over R, does not lead to a discrepancy between the corresponding calculated cross sections and experiment. The deviation of the rms radii obtained from different variants of the charge-density distribution from the mean amounts to approximately 1.5% and yields $\overline{R}$ = 3.4843 ± 0.038 F, which agrees with the values obtained on the basis of a phenomenological analysis with a Fermi density and a parabolic Fermi density.

To narrow down the possible error corridor of the charge-density distributions and to determine the details of their behavior in the central region of the nucleus, let us analyze the data II at large q. It is seen from Fig. 9 that here, too, there is an entire aggregate of charge-density distribution curves that are in sufficiently good agreement with experiment in the measured range of cross sections. In comparison with the first case, however, the corridor of the possible errors has become narrower, and this allows us to assess the qualitative variation of the charge-density distribution in the interior of the nucleus. The deviations from the rms radius for ^{40}Ca, as obtained from different charge-density-distribution variants, are already 0.8-1%, and $\overline{R}$ = 3.4792 ± 0.02 F, which agrees with the earlier results and the results of ref. 20.

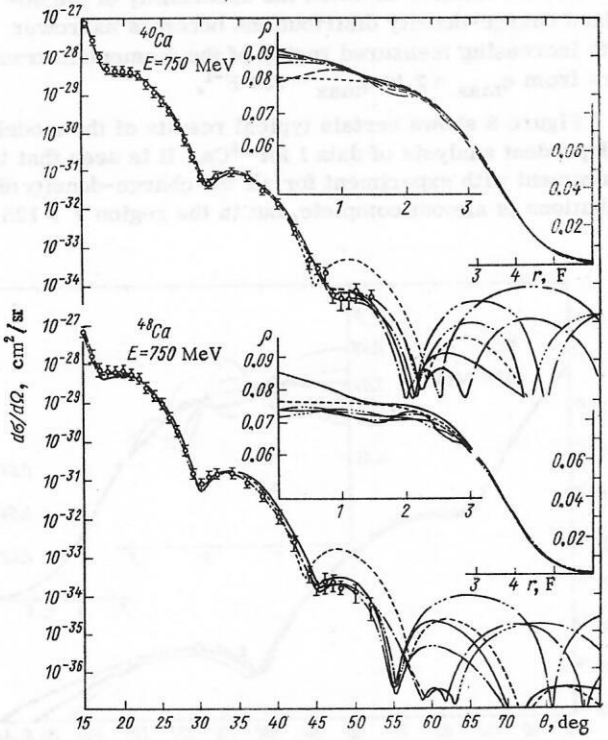

Fig. 9. Model-independent analysis of the elastic-scattering data of the Hofstadter group:[32] ——) calculated by that group; – – –) Fermi density; –·–, –··–, –···–, and –····–) densities that agree best in the model-independent analysis on the basis of the high-energy approximation.[30]

For the ^{48}Ca nucleus, the model-independent analysis yields charge-density distribution sets that differ in appearance and in form from the density obtained in ref. 32. Regardless of the choice of the input data, our method leads to charge-density distributions close to the Fermi density, but with a small oscillation in the region of F and with a more gently sloping surface fall-off. The rms radius in accord with the obtained set of charge-density distributions is $\overline{R}$ = 3.5198 ± 0.022 F, which agrees with the data of the phenomenological analysis of electron scattering[20] at 500 MeV on the basis of the parabolic Fermi density ($\overline{R}$ = 3.517 F).

Figure 10 shows the difference of the charge-density distributions of the nuclei ^{40}Ca and ^{48}Ca, multiplied by $4\pi r^2$, from which we gain an idea of their isotopic difference. The dash–dot curves correspond to the charge-density distributions of Fig. 9. The solid curve is the result of ref. 32, which predicted a negative isotopic shift of the charge-density distribution of ^{48}Ca relative to ^{40}Ca, and the dashed curve is the result of a theoretical calculation[33] that results in a relative increase of the rms radius on going from ^{40}Ca to ^{48}Ca, but in lower absolute values of the radii. Our analysis yields curves that lie between these two curves, and are more likely to be closer to the dashed curve.

Attempts were made to reconstruct the charge-density distributions on the basis of a model-independent analysis for other nuclei, and in each new investigation the trial charge-density distributions were chosen differently. The most thoroughly investigated nucleus is ^{208}Pb, for which, as already noted, a certain contradiction was observed between the phenomenological analysis data and the model calculations of the charge-density distributions. In the former, preference was given to a Fermi-like density with Gaussian asymptotic form, with a dip in the central region of the nucleus, while the latter (calculation by the Hartree–Fock method or by single-particle models) lead instead to a uniform rise of the charge-density distribution in the center of the nucleus. Although the model-independent analysis of the data on ^{208}Pb did not re-

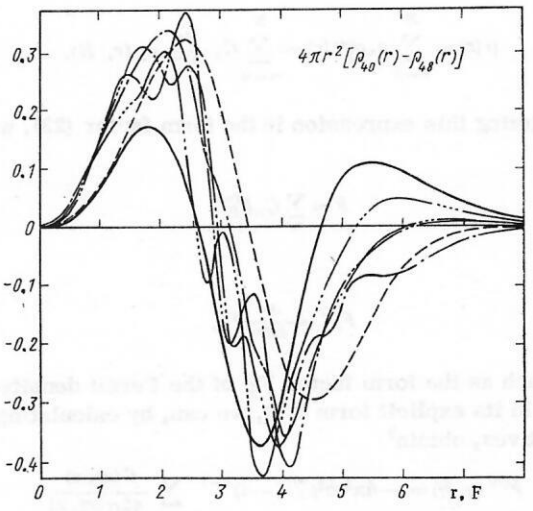

Fig. 10. Differences between the charge-density distributions of ^{40}Ca and ^{48}Ca: solid curves) from ref. 32; dashes) from ref. 33; dash–dot curves) from a model-independent analysis[30] and corresponding to the charge-density distributions of Fig. 9.

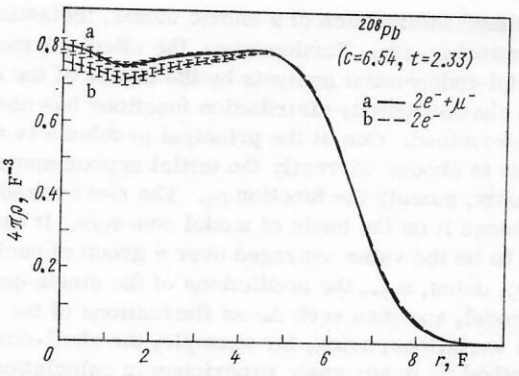

Fig. 11. Charge-density distributions obtained as a result of the model-independent analysis of data on electron scattering and of muon data (curves a) and of only electron data (curve b).[35]

solve this disparity, and the general conclusions of this analysis agreed in essence with those already drawn with the Ca isotopes as an example, we shall nevertheless describe these results briefly by way of illustration of the capabilities of the method.

Thus, in ref. 34 the model-independent analysis was carried for data at E = 124 and 167 MeV on the basis of the trial functions

$$\rho(r)=\sum_{i=1}^{N}\frac{p_i}{R_i^2}\delta(r-R_i), \tag{79}$$

where the charges of the p_i strips into which the nucleus was subdivided, its radii R_i, and the thicknesses $\Delta R = R/N$ were varied in a way as to make the spectrum of the possible charge-density distributions broad enough. As expected, the corridor of the possible charge-density distributions at these energies turned out to be very broad, so that it was impossible to give preference to any particular direction of the curves (with or without a dip in the center). In the same reference,[34] the permissible scatter of the charge-density distribution was analyzed with the aid of the moment functions

$$M(k)=\left(\int_0^\infty \rho(r)\,r^{k+2}\,dr\right)^{1/k}, \tag{80}$$

for which the uncertainty corridor was made narrower as a result of integration of $\rho(r)$ with weighting functions. It turned out that these data can lead to a definite conclusion concerning the course of the charge-density distributions only for the region $r \sim R$. To narrow down this corridor within the nucleus, $r < R$, and outside the nucleus, $r > R$, it is necessary to introduce model-dependent assumptions.

In another model-independent analysis of all the data on ^{208}Pb, including[35] the energy E = 500 MeV, use was made of the following radial-variation functions:

$$\Delta\rho=\sum_{n=1}^{N} C_n\frac{\sin(\pi nr/R)}{r}. \tag{81}$$

The Fermi density ρ_F was assumed for ρ_0. It turned out, naturally, that the uncertainty corridor at these energies became narrower. For the given form of the charge-density distribution, the shape of the curves inside the corridor recalls the bottom of a bottle (Fig. 11, curve b). This result is curious, although its authors cannot insist on it, since only a definite class of trial charge-density distributions was chosen for the analysis. Inclusion in the analysis of additional data on μ-mesic energies of this nucleus has narrowed down the uncertainties and smoothed out the course of the curves somewhat. This did not however, change, their qualitative behavior (curves a). In addition, all curves a went beyond the uncertainty corridor (curves b) of the charge-density distributions obtained from data on electron scattering only, this being due to inaccuracies in the allowance for radiative, dispersion, and other effects when the absolute experimental data were obtained. It is typical that in this model-independent analysis the scatter of the theoretical and experimental cross sections, $\Delta = (\sigma_{theor} - \sigma_{exp})/[(\sigma_{theor} + \sigma_{exp})/2]$, did not exceed ± 20% (Fig. 12).

In this respect, it is important to include in the model-independent analysis not only (and not so much) the

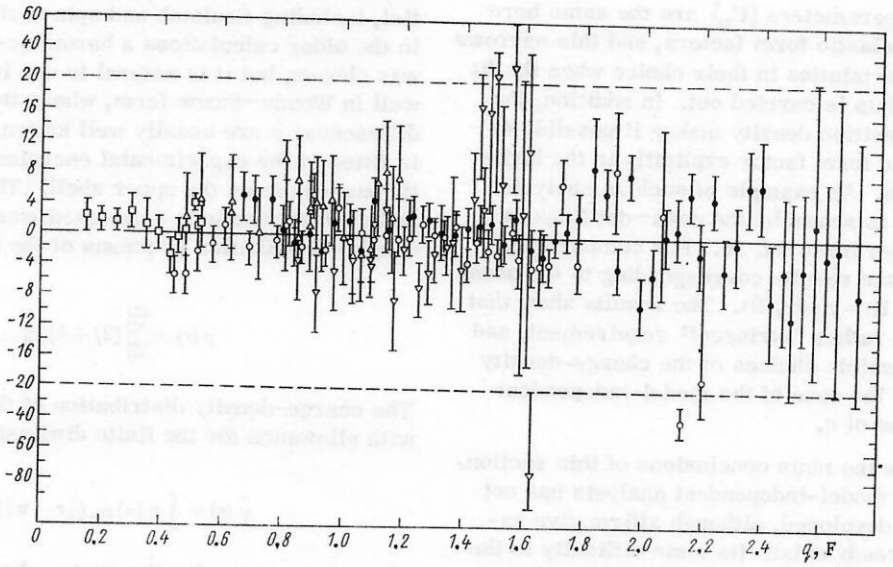

Fig. 12. Relative differences (in per cent) between the theoretical cross sections and the experimental ones obtained from a model-independent analysis of the electron-scattering and muon data.[35]

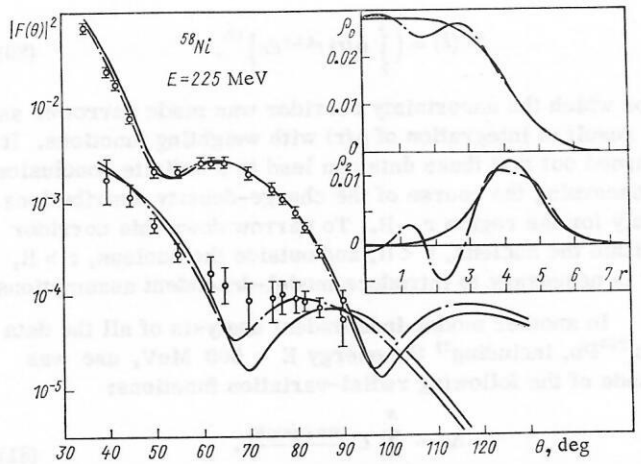

Fig. 13. Joint model-independent analysis of elastic and inelastic scattering (dash–dot) and calculations based on the Tassie macroscopic model with a Fermi density (solid curves).[36]

data on μ-mesic atoms, which are measured by a different procedure and can disagree for this reason alone with the (e, e) data, but also other data on electron scattering.

One such method was proposed in ref. 36, where data on inelastic scattering of electrons with excitation of the lowest 2^+ phonon state of ^{58}Ni were used together with the elastic-scattering data. In this case, an additional condition is imposed on the selection of the trial charge-density distribution curves, a condition that follows from rather general albeit model-dependent assumptions whereby the transition density $\rho_2(r)$ for this type of inelastic scattering is proportional to the first derivative of the charge density with respect to R:

$$\rho_2(r) \sim \frac{\partial}{\partial R}\rho(r,\ R). \tag{82}$$

Then, choosing the representation (74) for $\rho(r)$, we find that

$$\rho_2(r) \sim \sum_{n=0}^{N} C_n \frac{\partial^{n+1}}{\partial R^{n+1}}\rho_F(r,\ R). \tag{83}$$

The variational parameters $\{C_n\}$ are the same here for the elastic and inelastic form factors, and this narrows down greatly the uncertainties in their choice when the fit to the experimental data is carried out. In addition, the form (83) for the transition density makes it possible to calculate the inelastic form factor explicitly in the high-energy approximation. An example of such an analysis of the data of ref. 37 is shown by the dash–dot lines in Fig. 13, which is taken from ref. 36. For comparison, the solid lines show the results corresponding to the usual approach, when $\rho(r, R) = \rho_F(r, R)$. The results show that the relation (82) is a rather "stringent" requirement, and narrows down the possible choices of the charge-density distributions even in the case of the model-independent analysis at low values of q.

Let us formulate the main conclusions of this section. First, the method of model-independent analysis has not yet been completely developed, although affirmative examples of its use already exist. Its main difficulty is the large ambiguity of the charge-density distribution functions obtained. In this respect it is important to resort to additional information of μ-mesic atoms, inelastic electron scattering, etc. Furthermore, the effect exerted on the model-independent analysis by the choice of the class of trial charge-density distribution functions has not yet been determined. One of the principal problems is therefore how to choose correctly the initial approximation for the density, namely the function ρ_0. The most reasonable is to choose it on the basis of model concepts. It can be chosen to be the value averaged over a group of nuclei, $\rho_0 = \langle\rho\rangle$, using, e.g., the predictions of the single-particle shell model, and then seek $\Delta\rho$ as fluctuations of the radial density variations, using, for example, the shell-correction method.[38] In any case, experience in calculation of the charge-density distribution within the framework of some nuclear model can be quite useful here in the selection of the most realistic classes of trial charge-density distributions. We shall deal with these questions below.

Form Factors in the Independent-Particle Model

The simplest variant of charge-density distribution calculation is the one using the independent-particle model. This model makes it possible to analyze, albeit qualitatively, such questions as the appearance and character of the radial variations of the charge density distribution, the significance of the choice of the single-particle basis in the charge-density-distribution calculations and of the allowance for the residual interactions in the nucleus, the differences in the behavior of the form factors at large and small momentum transfers, etc. In addition, by resorting directly to a nuclear model we can attempt to describe simultaneously the data on nuclear structure and on scattering, for example, to explain, besides the form factors, the binding energies of the upper nuclear shells, the spectroscopic factors in direct nuclear reactions, etc. This narrows down greatly the possible ambiguities that arise in the charge-density distribution when the model-independent analysis treats only elastic electron scattering.

The usual procedure of calculating the charge-density distribution in accordance with the independent-particle model consists in the following: A single-particle potential, including Coulomb and spin–orbit forces, is chosen. In the older calculations a harmonic-oscillator potential was chosen, but it is natural to use in this problem a finite well in Woods–Saxon form, where the radius R and the diffuseness a are usually well known, and the well depth is fitted to the experimental energies required to detach the nucleon from the upper shell. The obtained proton radial wave functions ψ are used to calculate the charge-density distribution by means of the equation

$$\rho(r) = \sum_{nlj}^{(Z)} (2j+1)\,|\psi_{nlj}|^2. \tag{84}$$

The charge-density distribution of the nucleus is obtained with allowance for the finite dimensions of the proton:

$$\bar{\rho}(r) = \int \rho(u)\,\rho_p(|\mathbf{r}-\mathbf{u}|)\,d\mathbf{u}, \tag{85}$$

where we can use for the proton charge-density distribution ρ_p, for example, the parametrization of ref. 39.

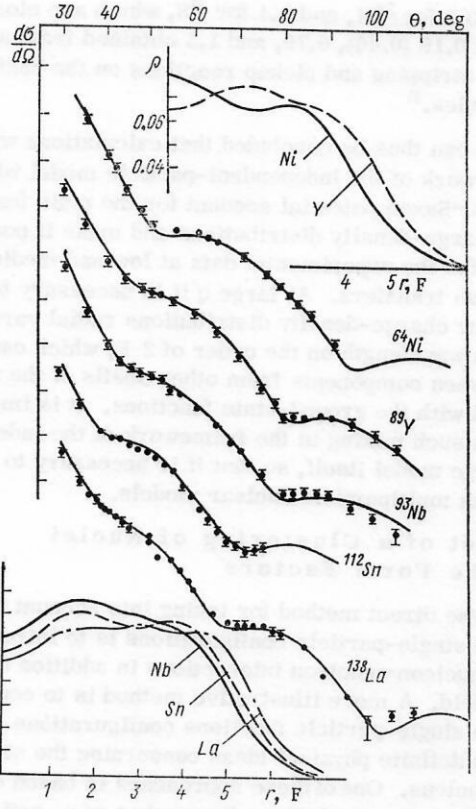

Fig. 14. Form factors of several nuclei, calculated on the basis of the charge-density distributions of the independent-particle model with a Woods–Saxon potential.[40]

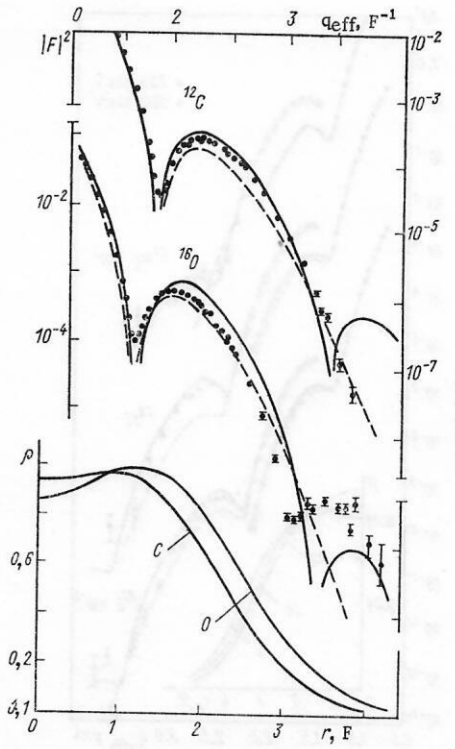

Fig. 15. Comparison of the experimental form factors with those calculated in the independent-particle model.[15]

As an example of the use of this procedure, we cite the calculation[40] of the charge-density distributions and form factors in the high-energy approximation for a number of nuclei with different atomic masses. The depth parameter of the corresponding Woods–Saxon potential was fitted to the binding energy of the proton from the upper shell. Figure 14 shows a comparison with experiment. It is seen that on the whole the agreement with experiment is satisfactory at low and medium momentum transfers, $q < 2\ F^{-1}$, thus indicating primarily the correct rate of decrease of the calculated charge-density distributions near the nuclear boundary. It turns out, further, that at the densities obtained the rms radii of the nuclei ^{58,60,64}Ni, ^{40,48}Ca, ^{89}Y, ^{93}Nb, ^{112,118}Sn, and ^{139}La lie in the ranges $\langle r^2\rangle^{1/2}/A^{1/3} = 0.95 \pm 30\%$; $\langle r^2\rangle^{1/2}/(2Z)^{1/3} = 0.99 \pm 10\%$, and their deviations from the mean values turn out to be even less than for the rms radii of the Fermi densities, corresponding to the best fit. This can serve as additional evidence favoring the conclusions of ref. 41, that the charge rms radii of the nuclei vary in proportion to $(2Z)^{1/3}$.

It is clear that at large q this simple approach of the independent-particle model is insufficient for calculation of the charge-density distributions. To verify this, we turn to the data on light nuclei, for which appropriate experiments and comparisons are available. As already noted, the Born approximation, which distinguishes a number of calculations, can be used for ^{12}C and in part for ^{16}O. Thus, the finite dimensions of the proton can be taken into account explicitly in the Born approximation. Substituting (85) in the form factor (68) of the nucleus, it is easy to separate from (68) the form factor of the proton, which takes the following form for a Gaussian density:

$$F_p(q) = \exp(-q^2\overline{R}^2(p)/2), \tag{86}$$

where $\overline{R}(p)$ is the rms radius of the proton. For light nuclei it is important to take into account also the motion of the center of the nucleus as a whole. In the oscillator basis, the variables of the single-particle motion and of the motion of the mass center are rather easy to separate.[42] As a result, taking (86) into account, we obtain a common correction factor G(q), with which it is necessary to multiply the square of the modulus of the theoretical form factor of the independent-particle model when the latter is compared with experiment:

$$G(q) = \exp[-q^2(\overline{R}^2(p) - \overline{R}^2(A)/A)/3]. \tag{87}$$

Figure 15 shows the results[15] of a comparison of the experimental form factors with those calculated in this manner for the p-shell nuclei ^{12}C and ^{16}O, using the traditional harmonic-oscillator model and a Woods–Saxon potential. We see that in the oscillator-potential approximation it is impossible to obtain even qualitative agreement with experiment at large q, since this approximation does not result in the second minimum obtained with a potential having a finite depth. It is interesting that for these nuclei the spin–orbit forces do not change the form factor significantly (the correction is of the order of 1%). Further, allowance for four-quasiparticle admixtures that result from inclusion of other nuclear shells likewise leads to no noticeable changes of the elastic form factors, although it does affect the inelastic ones. The general course of the charge-density

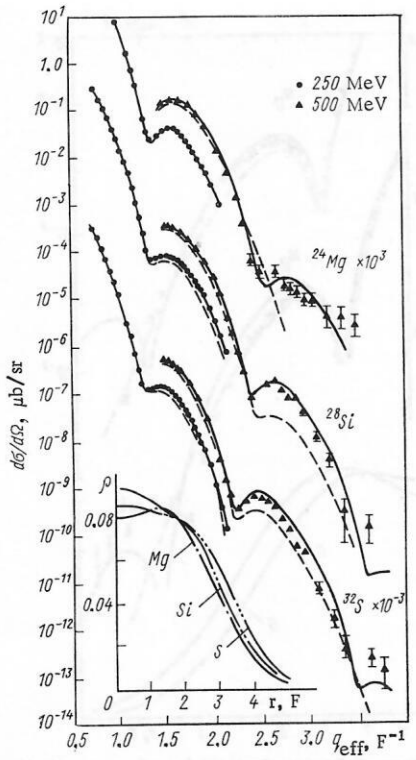

Fig. 16. Comparison of the experimental data and theoretical calculations by the independent-particle model in a harmonic-oscillator potential (dashes) and Woods–Saxon potential (solid curves), with occupation numbers introduced. The lower part shows the charge-density distributions corresponding to Woods–Saxon calculations.[43]

distributions obtained shows that, as expected, when the p-shell becomes filled, the density acquires a bump in the region $r \sim R$, where the functions of the 1p states have a maximum.

It is clear that to explain quantitatively the behavior of the form factors at large q it is necessary to improve the independent-particle model by introducing nucleon–nucleon correlations. This leads to such physical consequences as clustering, nuclear deformation, etc. In the wave function of the nucleus, this leads to a strong configuration mixing. This mixing, however, can be introduced formally, with the aid of occupation numbers that determine the admixture components. Let us consider in this connection, by way of example, the nuclei ^{24}Mg, ^{28}Si, and ^{32}S (ref. 43), where the $1d_5/2$ and 2s shells are being filled. According to the independent-particle model, the $1d_5/2$ shell is filled in ^{28}Si and the 2s shell is completely filled in ^{32}S. Since the 1d-state function has a maximum on the periphery of the nucleus, and the function of the 2s state has a maximum at the center, an abrupt rise of the charge-density distribution at the center of the nucleus (by approximately two times) should be observed on going from ^{28}Si to ^{32}S. An analysis of the experiment[43] shows, however, that this change is much smoother, starting with ^{24}Mg, and is the result of the influence of 2s admixtures to the functions of the 1d state. The corresponding calculation of the charge-density distributions and form factors within the framework of the independent-particle model, with introduction of the occupation numbers of the 2s shell, is shown in Fig. 16. A fit to the experimental results leads to the values 0.6 for ^{24}Mg, 0.9 for ^{28}Si, and 1.4 for ^{32}S, which are close to the values 0.19 (0.46), 0.79, and 1.5 obtained from an analysis of the stripping and pickup reactions on the basis of the sum rules.[44]

It can thus be concluded that calculations within the framework of the independent-particle model with a finite Woods–Saxon potential account for the main features of the charge-density distributions and make it possible to describe the experimental data at low and medium momentum transfers. At large q it is necessary to introduce into the charge-density distributions radial variations with a wavelength on the order of 2 F, which can appear only when components from other shells of the nucleus are mixed with the ground-state functions. It is impossible to obtain such mixing in the framework of the independent-particle model itself, so that it is necessary to use more perfect multiparticle nuclear models.

Effect of α Clustering of Nuclei on the Form Factors

The direct method for taking into account the mixing of the single-particle configurations is to introduce residual nucleon–nucleon interactions in addition to the average field. A more illustrative method is to construct out of the single-particle functions configurations corresponding to definite physical ideas concerning the structure of the nucleus. One of these approaches is based on the assumption of α clustering of a number of p- and sd-shell nuclei.[45] The simplest α model presupposes that the position of the α particles in the nucleus is strictly fixed, and antisymmetrization of the nucleons is not taken into account. By using this model it was possible to explain qualitatively the form factors of several light nuclei.[46] More consistent is the α-cluster model with projection (ACMP) or the Brink model.[47] Here the wave functions of the rotational nuclear states are generated out of an antisymmetrized multiparticle function constructed on the basis of a single-particle (usually Gaussian) function of the s states of nucleons that move relative to the α-clustering centers.

It should be noted that all scattering problems, including electron scattering, are quite sensitive to a shortcoming inherent in all multiparticle models, due to the use of the harmonic-oscillator function basis in these models. In this respect, the Brink multiparticle model is an exception, since it is possible to use in it, as shown in ref. 48, basis functions with realistic exponential asymptotic behavior.

The gist of the model is to separate in the nucleus the centers $\mathbf{R}_i$ ($i = 1, \ldots, N$ is the index of the cluster and N is the total number of clusters in the nucleus), where the α clusters are located. Relative to these centers, four nucleons are in s states with functions

$$u_a(\mathbf{r}-\mathbf{R}_i) = \chi_\sigma \chi_\tau u(|\mathbf{r}-\mathbf{R}_i|), \tag{88}$$

where $a = i, \sigma, \tau$ is the index of the single-particle state. A trial multiparticle antisymmetric function

$$U(\mathbf{R}) = \sum_p \varepsilon_p \prod_{a=1}^{A} u_a(pa) \tag{89}$$

is then constructed on the basis of (88) and used to make

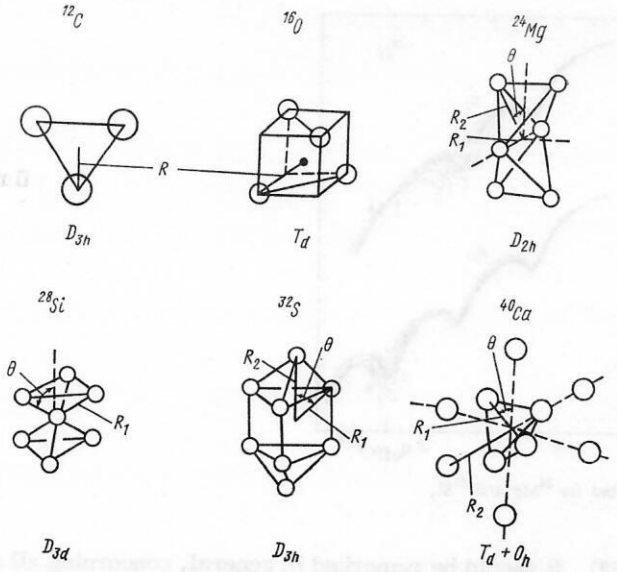

Fig. 17. Alpha configurations of p- and sd-shell nuclei, used in the form-factor calculations.

up, with the aid of the parity operator $\hat{P}_\pi$ and the projection operator $\hat{P}^J_{MK}$ (ref. 49), functions $|JMK\pi\rangle$ with specified quantum numbers, where K is the projection of the angular momentum J on the internal axis of the nucleus.

The complete function is the superposition

$$|JM\pi\rangle = \sum_K C^J_K |JMK\pi\rangle, \tag{90}$$

where the coefficients C^J_K for the lower states are determined from considerations of symmetry of the chosen α-particle configuration of the nucleus. These functions are used to calculate the matrix elements of the nuclear charge-density operator

$$\rho(\mathbf{r}, \xi) = \frac{1}{Z}\sum_{k=1}^{A} \varepsilon_k \delta(\mathbf{r}-\mathbf{r}_k) = \sum_{LM} \mathcal{F}_{LM}(r, \xi) Y^*_{LM}(\hat{r}), \tag{91}$$

where

$$\mathcal{F}_{LM} = \sum_{k=1}^{A} \mathcal{F}^{(k)}_{LM} = \sum_{k=1}^{A} \frac{\varepsilon_k}{Z} \delta(r-r_k) \frac{1}{r^2} Y_{LM}(\hat{r}_k).$$

It can be shown[48] that the charge-density distribution and the transition density (11) are equal in this case to

$$\rho_L = \frac{1}{4\pi^2 N^{1/2}_{00\pi_0}} \sum_K C^L_K N^{-1/2}_{LK\pi} \int d\theta \left[\langle U(\mathbf{R}) | \mathcal{F}_{LK} | U(\mathbf{S})\rangle + P_{\pi_0} \langle U(\mathbf{R}) | \mathcal{F}_{LK} | U(-\mathbf{S})\rangle\right], \tag{93}$$

where N are normalization factors of the wave functions. The integration is over the Euler angles and is due to the rotation, prescribed by the projection operator, from the initial α configuration of the nucleus $\mathbf{R} = \{\mathbf{R}_i\}$ to a new rotated configuration $\mathbf{S} = \{\mathbf{S}_i = \hat{\mathbf{R}}(\theta)\mathbf{R}_i\}$. The multiparticle matrix elements are expressed in terms of the determinants

$$\langle U(\mathbf{R}) | \mathcal{F}_{LK} | U(\varepsilon\mathbf{S})\rangle = 2[\det B_{ij}(\varepsilon)]^3 \sum_{n=1}^{A} \det B^{(n)LK}_{ij}(\varepsilon), \quad \varepsilon = \pm 1, \tag{94}$$

which are determined by the single-particle functions

$$B^{(n)LK}_{ij} = (u(\mathbf{r}-\mathbf{R}_i), \mathcal{F}^{(i)}_{LK} u(\mathbf{r}-\varepsilon\mathbf{S}_j))\,\delta_{ni} + B_{ij}(\varepsilon)(1-\delta_{ni}); \tag{95}$$

$$B_{ij}(\varepsilon) = (u(\mathbf{r}-\mathbf{R}_i), \quad u(\mathbf{r}-\varepsilon\mathbf{S}_j)). \tag{96}$$

Thus, from the technical point of view the problem consists of calculating first the single-particle matrix elements (95) and (96), and then the multiparticle elements (94), followed by three-dimensional integration in (93) over the Euler angles.

Naturally, the result depends on the choice of the geometrical configurations of the location of the α-cluster centers $\mathbf{R}_i$ and on the type of trial functions $u(\mathbf{r}-\mathbf{R}_i)$ used in the calculations. As to the α configurations, calculations of the characteristics of the ground states of a number of nuclei in accordance with the α-cluster model with projection,[47,50] and also calculations of the form factors by the α-particle model,[51] make it possible to choose the configurations in the form shown in Fig. 17. That is to say, an equilateral triangle for ^{12}C, a tetrahedron for ^{16}O, a bitetrahedron for ^{24}Mg, a D_{3d} structure for ^{28}Si, a D_{3h} structure for ^{32}S, and a tetrahedron inside an octahedron, $(T_d + O_h)$ structure, for ^{40}Ca. On the basis of the symmetries possessed by these figures we can find the coefficients C^J_K in the wave function (90). The single-par-

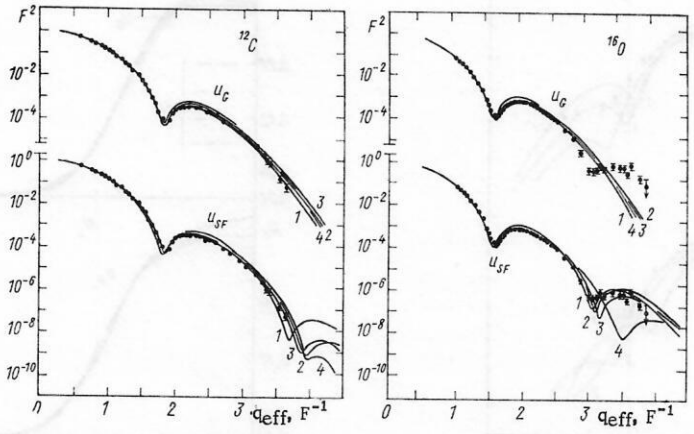

Fig. 18. Form factors of the nuclei ^{12}C and ^{16}O, calculated by the Brink model with Gaussian trial functions and with exponentially asymptotic functions for various sets of parameters.[52]

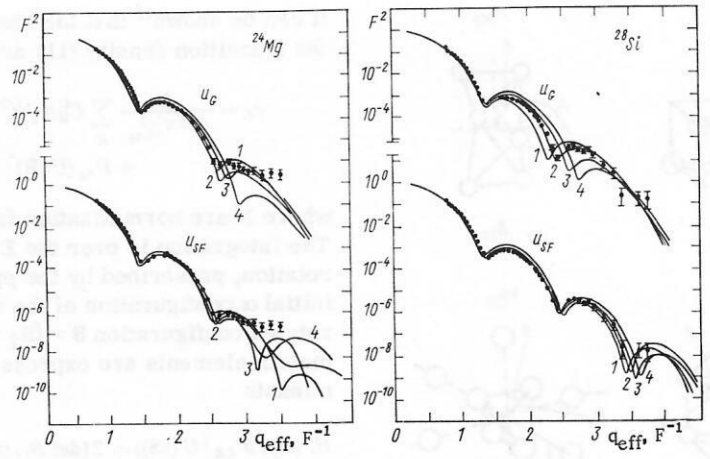

Fig. 19. The same as Fig. 18, but for ^{24}Mg and ^{28}Si.

ticle trial functions were chosen in refs. 48 and 52 in the traditional Gaussian form:

$$u_G(|\mathbf{r}-\mathbf{R}_i|) = \exp[-(\mathbf{r}-\mathbf{R}_i)^2/b_i^2] \qquad (97)$$

and in the form of functions with exponential asymptotic behavior:

$$u_{SF}(|\mathbf{r}-\mathbf{R}_i|) = [\mathrm{ch}(R_{\alpha i}/b_{\alpha i}) + \mathrm{ch}(|\mathbf{r}-\mathbf{R}_i|/b_{\alpha i})]^{-1}, \qquad (98)$$

where $R_{\alpha i}$ and $b_{\alpha i}$ determine the radius and width of the half-value region of the nucleon function around the center of the i-th α cluster. It turns out that the single-particle matrix elements with the functions (97) and (98) can be calculated in explicit form,[48] a highly valuable result for practical applications.

The results of the form-factor calculations in the high-energy approximation, performed in accordance with the described procedure, are shown in Figs. 18-21 (ref. 52). It should be remarked in general, concerning all nuclei, that the applicability of Gaussian trial functions are quite limited. Thus, calculations with these functions do not account for the features of the behavior of the form factors in the region of the second minimum of the p-shell nuclei and the third minimum of the d-shell nuclei. It is of interest to relate this behavior to the appearance of the diffraction minimum of the ^4He form factor at $q \sim 3.3$ F^{-1}. Indeed, the Gaussian charge-density distribution function $\rho(^4He) = \exp(-2r^2/b^2)$ cannot give a minimum in principle. At the same time, the function (98) with a realistic asymptotic form gives a density $\rho(^4He) = u_{SF}^2(r, R_i = 0)$ such that at R = 1.59 F and b = 0.545 F it is possible to explain not only the "size-effect" minimum of the free α particle, but also the entire variation of its experimental form factor.[48] It is therefore natural to assume that those "additional" minima or singularities at $q \sim 3$-3.3 F^{-1}, which are observed in the form factors of the indicated nuclei, are not the usual manifestation of the dimensions of the nucleus as a whole, but contain the features of the α-cluster structure inside the nucleus. At the same time, attempts[52] to describe the observed form factors of the nuclei ^{12}C, ^{16}O, and ^{28}Si with the parameters R and b of the free α particle and with a fit based only on the configuration pa-

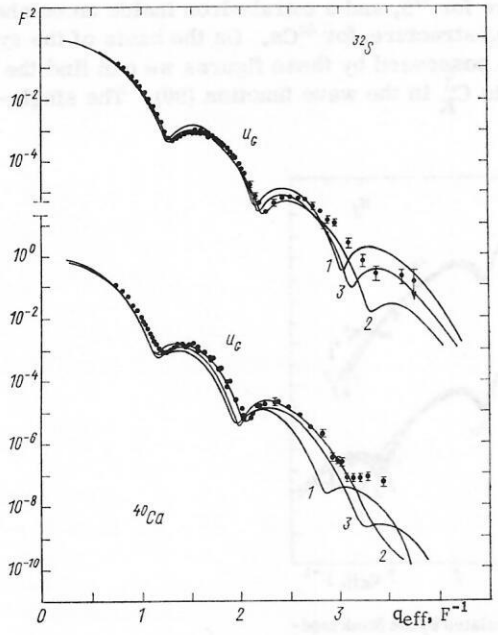

Fig. 20. Form factors of ^{32}S and ^{40}Ca. Calculation by the Brink model with Gaussian trial functions.[52]

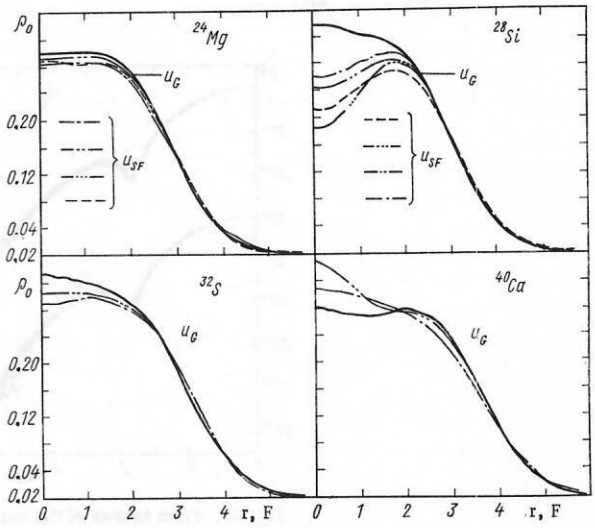

Fig. 21. Charge-density distributions corresponding to calculations on Figs. 19 and 20.

rameters R_i yielded no agreement at medium and large q. The only exception was ^{24}Mg, which can thus be regarded as being close to an α-particle nucleus. In the remaining nuclei, on the other hand, the α-cluster dimensions differ strongly from the α-particle dimensions.

The sets of parameters obtained for ^{12}C and ^{16}O show[48,50] that for ^{12}C the distance from the center of the nucleus to the α clusters is $R_i = 0.7$-1.1 F, i.e., it is quite small. Inasmuch as the alpha-cluster model with projection goes over into the shell model as $R \to 0$, this result can be regarded as indicating weak clustering of ^{12}C in the ground state. With respect to ^{16}O it can be concluded that it is not clustered at all in the ground state, since $R_i \approx 0$ for this nucleus. It is interesting that the clustering becomes more intense in the excited states of these nuclei.[48,52]

The comparison for ^{32}S and ^{40}Ca was made on the basis of Gaussian trial functions (see Fig. 20). The number of introduced parameters, determined by the configuration of the α clusters in the nucleus, increases in this case, so that the agreement obtained may not necessarily reflect at all times the physical picture of the true charge-density distribution in the nucleus (see Fig. 21).

The last conclusion concerns the observed ambiguity of the model description. Several sets of parameters, describing the experimental data with equal accuracy, are obtained for many nuclei. There are also sets that are close to those obtained in other studies[47,50] from variational calculations of the energies with nucleon–nucleon forces of various types. In this respect, the hope for successfully describing the form factors as criteria for the selection of NN-force variants has not yet been fulfilled. One can only emphasize once more the extent to which it is necessary to make use of data from other experiments in the analysis.

Short-Range Correlations in Nuclei and Form Factors

On going to large q, a natural idea[53] is that allowance must be made for the short-range correlations that appear between the nucleons of the nucleus as a result of repulsion at short distances. One of the simplest ways of introducing these correlations, the Jastrow method,[54] consists in parametrizing the wave functions of the nucleons of the nucleus relative to one another in such a way that they "fade out" when the distance between them becomes of the order of the nucleon "core." The fading function is specified phenomenologically and its parameters are determined by fitting to the experimental results, and the connection with the real nucleon–nucleon potential is not established. The second method is more complicated. It consists of introducing realistic or effective NN forces and solving numerically the nuclear multiparticle problem by the Hartree–Fock or by the more complicated Hartree–Fock–Bogolyubov method, in which long-range correlations of the nucleons of the nucleus are taken into account in addition to the short-range correlations.

We discuss first the results obtained in the Jastrow method.[55–57] The multiparticle function of the nucleus is expressed in this method in the form

$$\Psi(\mathbf{r}_1 \dots \mathbf{r}_A) = \Phi(\mathbf{r}_1 \dots \mathbf{r}_A) \prod_{i<j}^{A} F(r_{ij}), \tag{99}$$

where

$$\Phi(\mathbf{r}_1 \dots \mathbf{r}_A) = \sum_p \varepsilon_p \frac{1}{A^{1/2}} \prod_{a=1}^{A} u(pa) = \frac{1}{A^{1/2}} \det\{u_p\} \tag{100}$$

is the usual Slater determinant made up of single-particle functions. F(r) is parametrized to take into account the short-range repulsion of the nucleons at short distances, e.g., $F^2(r) = 1 + h(r)$; $h(r) = \exp(-r^2/b^2)$. Here b is a parameter that determines the fall-off rate at short distances. Substituting (99) in expression (68) for the Born form factor, with the charge-density distribution of the nucleus given in the form of a sum of point-like charges (91):

$$F^p(q) = \frac{1}{A} \left\langle \Psi \left| \sum_{j=1}^{A} \exp(i\mathbf{q}\mathbf{r}_j) \right| \Psi \right\rangle, \tag{101}$$

we can, using the cluster-expansion method[58] and retaining only the zero- and first-order terms in the pair correlation function h(r), express the form factor in terms of single-particle matrix elements:[55]

$$F^p(q) = \frac{1}{A} \Big\{ \sum_i \langle i | j_0(qr_1) | i \rangle - \sum_{ij} \langle ij | j_0(qr_1)\, h(r_{12}) | ij - ji \rangle - \sum_i \langle i | j_0(qr_1) | i \rangle \sum_{kl} \langle kl | h(r_{12}) | kl - lk \rangle \Big\}. \tag{102}$$

We recall that the measured form factor is $|F(q)|^2 = G(q)|F^p(q)|^2$, where G(q) takes into account the nucleon dimensions and the motion of the mass center of the nucleus (87). The problem consists thus of separating the variables in (102) and carrying out the corresponding integrations. The difficulties in the problem of separating the variables make it necessary usually to resort to the harmonic-oscillator basis functions, for which the Talmi–Moshinsky transformation is used to change over to the relative-motion variables. It is then necessary to forego the correct asymptotic form of the single-particle functions. Figure 22 shows a typical example of such calculations[55] for the light nuclei ^4He, ^6Li, ^{12}C, and ^{16}O. Good agreement with experiment is seen and, more interestingly, it is possible to obtain by this method the second minimum in the form factors of the p-shell nuclei, a minimum distinctly observed in ^{16}O. It can thus be concluded that the Jastrow method accounts for the real features of the charge-density distribution, in spite of the fact that the calculation is based on basis functions that do not have the correct asymptotic form. A characteristic fact is that allowance for the short-range correlations leads to a weakening of the contribution of the single-particle functions to the charge-density distribution in the central part of the nucleus and an increase of this density on the periphery of the nucleus.

The calculation of (102) with finite-potential functions is a rather difficult task, and special methods must be developed to separate the variables, and particularly to single out the variables of the mass center of the nucleus. Nonetheless, calculations by the Jastrow method, using Woods–Saxon potentials, have already been made.[57] Comparing these two approaches and the results of their com-

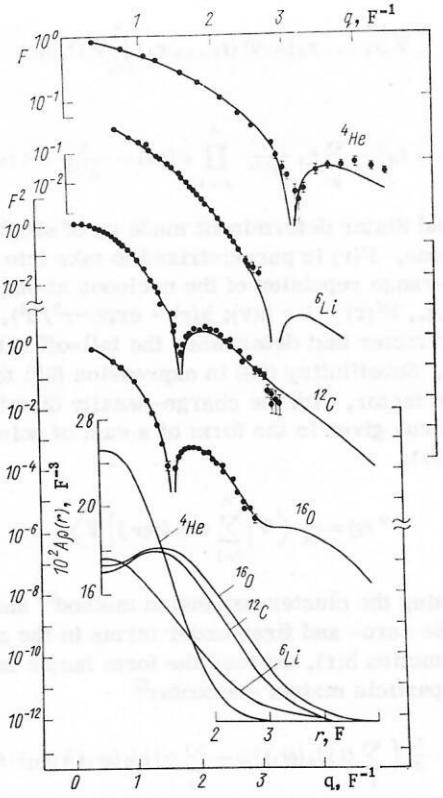

Fig. 22. Form factors of light nuclei and the corresponding charge-density distributions calculated with allowance for the short-range repulsion of the nucleons (harmonic-oscillator basis functions).[55]

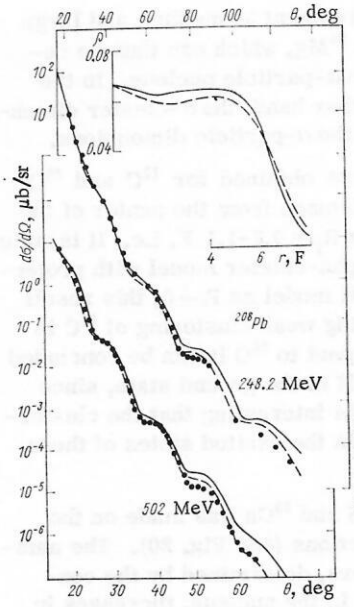

Fig. 23. Charge-density distribution of ^{208}Pb, calculated by the Hartree–Fock method, and the corresponding form factors.[60]

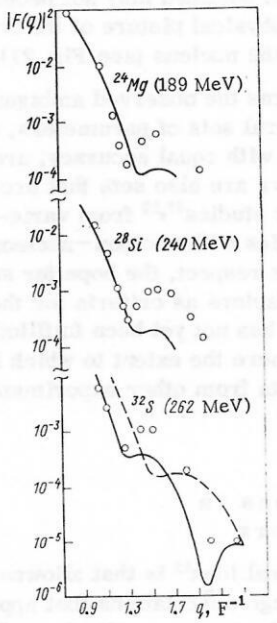

Fig. 24. Form factors of sd-shell nuclei calculated by the Hartree–Fock method. Solid curves) harmonic-oscillator basis; dashes) Woods–Saxon potential functions basis.[61]

parison with experiment, we can conclude that introduction of short-range correlations into multiparticle functions constructed on a basis of single-particle functions of a finite well can improve the quantitative agreement with experiment in the region of large q. Since the question of estimating this contribution is connected in many respects with some leeway in the choice of the single-particle basis, it is still impossible to answer conclusively the question of the true significance of the short-range correlations in this momentum region. It is perfectly possible that the effect of the short-range correlation is accounted for in many respects by introducing an average field – a potential of finite depth.

From among the numerous calculations of the charge-density distributions and of the other characteristics of the nucleus by the self-consistent field method, we present here only two examples: 1) Calculation by the Hartree–Fock method, which has recently become quite popular and economic, owing to the introduction of Skyrme's effective NN potential.[59] In this potential the short-range repulsion of the nucleons and the dependence on the density of the nucleus are taken into account in a very simple manner, and this is equivalent to taking three-particle forces into account. Figure 23 shows a typical illustration of calculation,[60] performed by this method, of the form factor of the ^{208}Pb nucleus for two types of Skyrme potential. Good agreement with experiment is obtained up to the maximum momentum transfer. It is interesting that the corresponding charge-density distributions do not agree with the behavior predicted by the phenomenological charge-density distribution function with Gaussian asymtotic form (cf. Fig. 6). Typical of Hartree–Fock calculation is the use of an oscillator basis. 2) A calculation[61] that can be classified as a Hartree–Fock calculation only arbitrarily. It consists of using multiparticle trial functions obtained by projecting the rotation from the determinant of the basis functions of the deformed field. The basis functions themselves were chosen both in an oscillator potential and in a Woods–Saxon potential.

Some results of such calculations for 2s–1d shell nuclei are shown in Fig. 24. In view of the limited character of the chosen basis, and since there are difficulties of principle when it comes to take into account the nonbound states in a Woods–Saxon potential, the comparison with experiment is only qualitative. Nonetheless, it is from the figure that the advantages of finite-well functions begin to manifest themselves with increasing momentum transfer.

Thus, summarizing the results of the "model comparisons," we can draw the general conclusion that there

exists a model ambiguity of sorts when it comes to describing the elastic-scattering form factors, i.e., almost each model, once brought to a certain degree of perfection, describes adequately the charge form factors at practically all observed values of the momentum transfer, including large q. This result is, on the one hand, the consequence of much work performed in recent years to improve the models, and the other hand stimulates a search for new data, e.g., the analysis of inelastic scattering, so as to establish with the aid of the aggregate of the numerous comparisons the advantages of the initial premises on which a particular nuclear model is based.

It can be stated with assurance, nevertheless, that methods and models based on the use of oscillator-potential functions call, as a rule, for the introduction of additional assumptions, interactions, etc., which in final analysis make it possible to correct simply the asymptotic forms of these functions. The description of the experimental data becomes more natural if the calculations are based on functions having the correct exponential asymptotic behavior.

3. INELASTIC SCATTERING OF ELECTRONS WITH EXCITATION OF LOW-LYING COLLECTIVE NUCLEAR LEVELS

The inelastic scattering of electrons by nuclei yields valuable information on the structure of the nucleus. Besides the reduced transition probability, which can be separated in some cases from such cross sections, the very form of the angular distribution is connected with the multipolarity of the transition and is quite sensitive to the form of the radial transition density (21). In addition, the inelastic-scattering data yield further information, the analysis of which, in conjunction with elastic-scattering data, makes it possible to formulate more rigorous limitations on the choice of the charge-density distribution and the radial transition density in the procedure of the model-independent search or else, as a result of direct model calculations and comparisons with experiments, will reveal the best founded nuclear models.

Just as in the case of elastic scattering, the inelastic form factors can be calculated by using the Born approximation for light nuclei, and the exact phase-shift analysis method or the high-energy approximation for heavy nuclei. We presented above a general expression (23) for the inelastic-scattering form factor in the high-energy approximation, expressed in terms of integrals of the radial transition-density functions $\rho_L(x)$. The latter can be calculated independently in any model of the nucleus. Below, following ref. 36, we shall show how to calculate the corresponding form factors in an explicit analytic form by using the characteristic general properties of the radial transition density with excitation of low-lying collective nuclear levels. We next describe in detail how to calculate the radial transition densities within the framework of macroscopic and microscopic models of the nucleus. Particular examples of the calculation of inelastic form factors and their comparison with experiment, as well as some general conclusions, will be given below.

Inelastic Form Factors in the High-Energy Approximation

We calculate the integral (23), which determines the inelastic-scattering form factor, in general form for an arbitrary form of the radial transition density $\rho_L(x)$. To this end, we focus our attention on a characteristic feature in the behavior of the radial transition densities in single-phonon transitions, namely, all have a maximum in the region of the nuclear boundary ($x \approx R$), fall off exponentially in the outer region ($x > R$), and undergo a number of oscillations inside the nucleus ($x < R$). It is possible to use for functions of this type a method developed in refs. 9 and 36. It consists in representing a Fermi-like function as a series of derivatives of a Fermi density. In our case we have

$$\rho_L(x) = \sum_{m=0}^{N} a_m^L \phi^{(m)}(x;\ R,\ b); \tag{103}$$

$$\phi^{(m)}(z) = \frac{d^m}{dz^m}\phi^{(0)}(z) = \frac{d^m}{dz^m}\cdot\frac{1}{1+e^z}\left(z=\frac{x-R}{b}\right). \tag{104}$$

It is easiest to find here the expansion coefficients a_m^L and the number N of terms in the series by a least-squares fit of the series (103) to the specified function $\rho_L(x)$. The expansion (104) thus becomes fully defined. Substituting it in (23), where we interchange the integration and differentiation, and using the pole method of evaluating the integrals obtained, we get

$$F_{L0}(q,E) = \sum_{m=0}^{N} a_m^L I_{L0}^{(m)}(q,E), \tag{105}$$

where

$$I_{L0}^{(m)}(q,E) = 4\pi^2 q b^2 (-\mathrm{i})^{m-1} \sum_{\varepsilon=\pm1} \frac{G_{L0}(x_0^\varepsilon)}{q_{\mathrm{eff}}^2(x_0^\varepsilon)} \times (bq_{\mathrm{eff}}(x_0^\varepsilon))^{m-1}\,[m + q_{\mathrm{eff}}(x_0^\varepsilon)\,(\mathrm{i}R - \varepsilon\pi b\,\mathrm{cth}\,\pi qb)] \times \frac{\exp \mathrm{i}\,[\varepsilon qR + \phi(x_0^\varepsilon)]}{2\,\mathrm{sh}\,q\pi b}.$$

Here $x_0^\varepsilon = R + \mathrm{i}\,\varepsilon\pi b$; the functions $\phi(x)$, $q_{\mathrm{eff}}(x)$, and $G_{L_0}(x)$ are known in explicit form and are given in Appendix 1. If L = 0 this result coincides with the previously obtained expression[9] for elastic scattering with an arbitrary charge-density distribution $\rho_0(x)$. It is easy to generalize this result to include the case $M \neq 0$, but this leads to a small increment on the order of $(qR)^{-2}$.

Thus, the problem of calculating the inelastic-scattering cross section has now been reduced to expanding the radial transition density obtained by some model into the series (103) and using the obtained coefficients a_m^L to calculate the integral (105), which determines the inelastic-scattering cross section.

Transition Density in the Macroscopic Model

In this case the radial transition density is usually found on the basis of the Fermi density $\rho_F(x, R, b)$ of the nucleus, where the parameter R is regarded as a function of the dynamic variables $\alpha_{\lambda\mu}$ that characterize the oscillations of the nuclear surface about the equilibrium spherical shape, namely

$$\rho_F(xR_0b) = \rho_0\{1 + \exp([x - R_0 - \Delta R(\Omega)]/b)\}^{-1}, \tag{106}$$

where

$$\Delta R(\Omega) = R_0 \sum_{\lambda\mu} \{\alpha_{\lambda\mu} Y_{\lambda\mu}(\Omega) - [(-1)^{\mu}/4\pi]\,\alpha_{\lambda\mu}\alpha_{\lambda-\mu}\};$$

Ω are the angular coordinates of the moving electron. Now expanding ρ_F in terms of the small quantity $\Delta R/R_0$ and retaining the first nonvanishing terms in each transition, we obtain for the radial density of the transition $\rho_L^{(n)}(x)$ from the ground state of the nucleus $|0\rangle$ to the excited state $|n, JM\rangle$ (n is the number of phonons) the following expressions:

1) for the ground state (n = 0, elastic scattering):

$$\rho_L^{(0)}(x) = \rho_F^{(0)}(x) \cdot \langle 0 \| \delta_{L0} \| 0\rangle; \tag{107}$$

2) for a one-phonon transition (n = 1, L = 2,3), in the Tassie model:[62]

$$\rho_L^{(1)}(x) = \langle J;\ 1 \| \hat{\mathfrak{M}}_L \| 0\rangle \frac{1}{J_L^{(1)}} \rho_F^{(1)}(x); \tag{108}$$

3) for a two-phonon transition (n = 2, L = 2,4,...):

$$\rho_L^{(2)}(x) = \langle J;\ 2 \| \hat{\mathfrak{M}}_L \| 0\rangle \frac{1}{J_L^{(2)}} \rho_F^{(2)}(x); \tag{109}$$

4) for monopole transitions (n = 2, L = 0):

$$\rho_0^{(2)}(x) = \langle 0;\ 2 \| \hat{\mathfrak{M}}_0 \| 0\rangle \frac{1}{J_0^{(2)}} [\rho_F^{(1)}(x) - R\rho_F^{(2)}(x)], \tag{110}$$

where

$$J_{L\neq 0}^{(n)} = \int \rho_F^{(n)}(x)\, x^{L+2}\, dx; \quad J_0^2 = R^3 \int [\rho_F^{(1)}(x) - R\rho_F^{(2)}(x)]\, x\, dx; \tag{111}$$
$$\rho_F^{(n)}(x) = \frac{\partial^n}{\partial(\Delta R)^n} \rho_F(\mathbf{x}, R_0, b)\,|_{\Delta R=0},$$

and $\mathfrak{M}_L$ is the operator of the electric and monopole (L = 0) transitions.

Using the definition of the reduced transition probability[63]

$$B^{(n)}(EL;\ J \to 0) = |\langle J;\ n \| \hat{\mathfrak{M}}_L \| 0\rangle|^2, \tag{112}$$

we thus obtain the following expression for the scattering cross section:

$$\left(\frac{d\sigma}{d\Omega}\right)_{i\to f}^{(n)} = \left(\frac{d\sigma}{d\Omega}\right)_{\text{Mott}} \cdot \frac{2J_i+1}{2J_f+1} \sum_{LM} \frac{1}{e^2} B^{(n)}(EL;\ J_f \to J_i)\ \frac{|F_{LM}^{(n)}|^2}{2L+1}. \tag{113}$$

Here

$$F_{LM}^{(n)}(q,E) = \frac{1}{J_L^{(n)}} \sum_{m=0}^{N} a_m^{(n)} I_{LM}^{(m)}(q,\ E), \tag{114}$$

where we have respectively in the case of single-phonon, two-phonon, and monopole transitions: $a_m^{(n)} = (1/b^n)\delta_{mn}$; $a_m^{(0)} = [\delta_{1m}/b - R\delta_{2m}/b^2]$.

It should be noted that the traditional approach to inelastic scattering, based on a hydrodynamic description of the oscillations or rotations of the nucleus, is most convenient for the reduction of the experimental data. What is analyzed in this case is only the kinematic part of the cross section, which describes the angular distribution, while the comparison of the absolute values of the cross sections gives the reduced probability of an electric transition of multipolarity L. It is possible, however, to generalize this approach somewhat, with account taken, at least formally, of certain characteristic features of the charge-density distributions (their "fine" shell structure); these characteristics have become known in recent years. On the other hand, calculations of charge-density distributions and of radial transition densities on the basis of microscopic nuclear models always yield radial variations of similar type, and their behavior conforms in the main to that described above. Namely, the transition density of a one-phonon transition is quite close to the derivative of the charge density. All this allows us to construct a unified phenomenological description of elastic and inelastic electron scattering on the basis of a single charge-density distribution of arbitrary form:

$$\rho(x) = \sum_{m=0}^{N} a_m \phi^{(m)}(x;\ R,\ b). \tag{115}$$

In this case the functions $\rho^{(n)}(x)$ (n = 1, 2) from Eqs. (107)-(114) acquire a more general meaning, wherein they are now derivatives of the charge-density distributions (115) and are expressed in terms of the same coefficients:

$$\rho^{(n)}(x) = \frac{1}{(-b)^n} \sum_{m=0}^{N} a_m \phi^{(m+n)}(x;\ R,\ b). \tag{116}$$

Although this generalization is somewhat formal, it is valid to the same degree (i.e., it violates the principles of the hydrodynamic model of the nucleus) that the traditional scheme described above is valid. On the other hand, this generalization can be used in the model-independent analysis of the experimental data, for the purpose of extracting information on the charge-density distributions. This analysis can now be carried out simultaneously for elastic and inelastic scattering using expression (115) for the charge-density distribution and (116) for the radial transition density with the same set of coefficients a_m, which are found as variable parameters when theory and experiment are compared by the χ^2 method. This simultaneous analysis can reduce the uncertainty in the variation of the charge-density distribution in the interior of the nucleus, i.e., the uncertainty obtained when only the elastic-scattering data are analyzed at the usual electron energies (see Fig. 13).

Transition Density and Microscopic Models

In the microscopic model, the variables ξ describing the states of a spherical nucleus are the operators $a_{\nu\tau}^{+}$ and $a_{\nu\tau}$ for the creation and annihilation of a particle in the state ν = n, l, j, m with isospin projection τ. In terms of these operators, the charge-density distribution takes the following form common to all microscopic models:

$$\rho(\mathbf{x}\xi) = \sum_{n=1}^{A} \rho(\mathbf{x} - \mathbf{r}_n) = \sum_{\nu_1\nu_2\tau_1\tau_2} \langle \nu_1\tau_1 |\, \rho(\mathbf{x}-\mathbf{r})\, | \nu_2\tau_2\rangle\, a_{\nu_1\tau_1}^{+} a_{\nu_2\tau_2}. \tag{117}$$

The wave functions $|\nu\tau\rangle$ of the basis are defined by

$$\left.\begin{aligned} |\nu\tau\rangle &= R_{\bar{\nu}}(r)\, \chi^{\tau} i^{l} \left| l\,\tfrac{1}{2}\, jm \right\rangle; \\ \left| l\,\tfrac{1}{2}\, jm \right\rangle &= \sum_{\mu} \left(l\,\tfrac{1}{2}\,\mu,\ m-\mu \,|\, jm \right) Y_{l\mu}(\hat{r})\, \chi_{1/2}^{m-\mu} \\ &(\bar{\nu} = n,\ l,\ j). \end{aligned}\right\} \tag{118}$$

For point charges we have

$$\rho(\mathbf{x}-\mathbf{r}) = \varepsilon_\tau \delta(\mathbf{x}-\mathbf{r}) = \varepsilon_\tau \frac{\delta(x-r)}{x^2} \sum_{LM} Y_{LM}(\hat{r})\, Y^*_{LM}(\hat{x}),$$

and then

$$\rho(\mathbf{x}\xi) = \sum_{LM} \mathscr{P}_{LM}(x, \xi)\, Y^*_{LM}(\hat{x}),$$

where

$$\mathscr{P}_{LM} = \sum_{\bar{\nu}_1\bar{\nu}_2\tau} A^L_{\bar{\nu}_1\bar{\nu}_2\tau}(x)\,[a^+_{\bar{\nu}_1\tau} a_{\bar{\nu}_2\tau}]_{LM};$$

$$A^L_{\bar{\nu}_1\bar{\nu}_2\tau}(x) = \varepsilon_\tau R_{\bar{\nu}_1}(x)\, R_{\bar{\nu}_2}(x)$$

$$\times i^{l_1-l_2-1}(-1)^{j_1}\sqrt{(2j_2+1)/4\pi}\left(j_1 j_2 \tfrac{1}{2} -\tfrac{1}{2}\middle| L0\right);$$

$$[a^+_{\nu_1\tau} a_{\nu_2\tau}]_{LM} = \sum_{m_1 m_2} (j_2 L m_2 M \mid j_1 m_1)\, a^+_{\nu_1\tau} a_{\nu_2\tau}.$$

Thus, the radial transition density is expressed in general form by

$$\rho_L(x) = \langle J_f \| \mathscr{P}_L(x, \xi) \| J_i\rangle = \sum_{\bar{\nu}_1\bar{\nu}_2\tau} A^L_{\bar{\nu}_1\bar{\nu}_2\tau}(x)\,\langle J_f \| [a^+_{\nu_1\tau} a_{\nu_2\tau}]_{LM} \| J_i\rangle, \qquad (119)$$

where $|J_{i,f}\rangle$ are the wave functions of the ground (i) and excited (f) states of the nucleus and are defined within the framework of some concrete microscopic model.

The expression (119) for point-like particles can be generalized to the case when the nucleus have a smeared-out charge with density $\rho_p(x)$. Then the radial transition density $\bar{\rho}_L(x)$ is defined as follows:

$$\bar{\rho}_L(x)\, Y^*_{LM}(\hat{x}) = \int \rho_L(r)\, Y^*_{LM}(\hat{r})\, \rho_p(|\mathbf{x}-\mathbf{r}|)\, d\mathbf{r}. \qquad (120)$$

It is of interest to verify the method proposed above for calculating inelastic scattering with the corresponding exact calculations, using the same microscopic model of the nucleus as a basis. Exact calculations of this kind were performed in ref. 28, where inelastic scattering of electrons by spherical nuclei was considered, and the wave functions of the relative motion of the electron were obtained by numerically solving the Dirac equation, while the low-lying excited states were regarded as phonon states on the basis of a microscopic nuclear model with account taken of the residual pair and quadrupole interactions of the nucleus. Models of this type are frequently employed of late, but in ref. 28 there were introduced certain modifications needed in order to consider questions connected with scattering. Namely, the single-particle basis (118) was chosen in the form of functions in the field of a Woods–Saxon potential with $\mathbf{l}\cdot\mathbf{s}$ terms included. This gives the correct (experimental) asymptotic form of these functions and of the corresponding charge-density distributions and radial transition densities in the region of the nuclear boundary, a factor of importance in the description of elastic and inelastic scattering.

This model yields for the transition to the single-phonon state $|JM\rangle = B^+_{JM}|0\rangle$, in agreement with ref. 28, the following expression for the radial transition density:

$$\rho_L(x) = \sum_{\substack{\nu_1\bar{\nu}_2\tau \\ (j_1\le j_2)}} (1+\delta_{\bar{\nu}_1\bar{\nu}_2})^{-1/2} (v_{\bar{\nu}_1\tau} u_{\bar{\nu}_2\tau} + v_{\bar{\nu}_2\tau} u_{\bar{\nu}_1\tau})$$

$$\times (\Pi^{\bar{\nu}_1\bar{\nu}_2\tau}_L - \Lambda^{\bar{\nu}_1\bar{\nu}_2\tau}_L)\, A^L_{\bar{\nu}_1\bar{\nu}_2\tau}(x). \qquad (121)$$

Here (u, v) and (Π, Λ) are the amplitudes of the quasiparticle and phonon transformations.

Comparison with Experiment

So far, the Tassie phenomenological model is one of the most popular radial transition density models, and is used for the analysis of inelastic scattering of electrons by nuclei with excitation of the lowest single-phonon levels. The purpose of this analysis is usually to obtain with the aid of (113) exact information (in view of the electromagnetic character of the interaction) on the transition probabilities B(EL) and the main characteristics of the size of the nuclear region where the transition is effected, such as its "centroid" R and its "width" b. Since the lowest derivatives of the Fermi density, which determine the radial transition density functions in the phenomenological approach, do not contain fast variations of the shell type, it follows that models of this type can claim agreement with experiment only at low and medium momentum transfers.

By way of example we present the results of an analysis[64] of earlier experimental data[65] on inelastic electron scattering by the nucleus ^{52}Cr, with excitation in this nucleus of a single-phonon 2^+ state or two two-phonon states 2^{2+} and 0^+ (Fig. 25). The calculation was carried out in the high-energy approximation, and the parameters R and b were fixed in ref. 8 in accordance with the data on the elastic scattering by the same nucleus. A comparison of the experimental and theoretical cross sections (113) has made it possible to determine the corresponding B(EL). A comparison of the calculations in the high-energy approximation and in the Born approximation shows that the distortion effects are of important significance and yield not only the shift and the filling of the diffraction minima, but also alter the absolute values of the cross sections, which is of importance when it comes to obtaining exact information on B(EL).

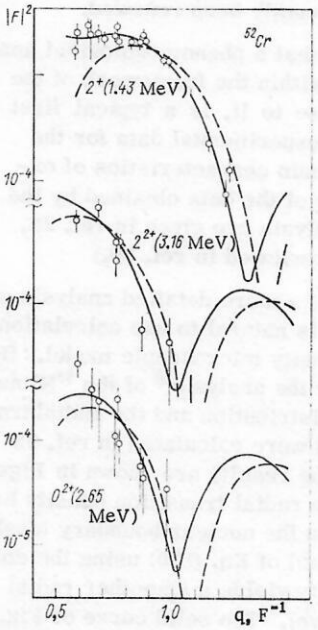

Fig. 25. Form factors of inelastic electron scattering by ^{52}Cr, calculated in the Tassie macroscopic model: solid curves) high-energy approximation; dashes) Born approximation.[64]

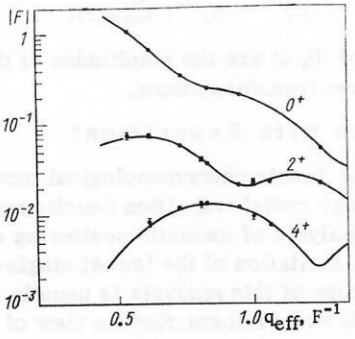

Fig. 26. Inelastic electron scattering by ^{152}Sm with excitation of levels of the ground rotational bands. Calculation by the macroscopic model.[66]

Recently, following the appearance of data on scattering from deformed nuclei, this model came into use for the determination of the main characteristics of such nuclei, namely the deformation parameters β_L. Thus, the inelastic scattering of electrons by ^{152}Sm with excitation of the levels 0^+, 2^+, and 4^+ of the ground rotational band was analyzed in ref. 66 (Fig. 26). The Tassie model was generalized there in such a way that account was taken of the higher-order corrections for the possible nuclear deformation:

$$\Delta R = R_0 (1 + \beta_2 Y_{20}(\Omega) + \beta_4 Y_{40}(\Omega) + \beta_6 Y_{60}(\Omega)). \qquad (122)$$

By optimal fitting, the following values were obtained: $\beta_2 = 0.287$ and $\beta_4 = 0.070$ (the parameter β_6 was taken from data on α-particle scattering, $\langle r^2 \rangle^{1/2}$ was taken from μ-mesic atom data, and B(E2) was known). It should be noted, however, that in addition to the increase of the diffuseness parameter, an important role in the scattering by deformed nuclei[24] with excitation of rotational-band levels is assumed also by effects of higher order of perturbation theory, namely multiple scattering, as pointed out in ref. 67. It should also be easy to excite in deformed nuclei β- and γ-vibrational levels, for which the corresponding form factors can be calculated[68] within the framework of the Davydov phenomenological models. Interest in this question has recently been renewed.

It can thus be concluded that a phenomenological analysis of inelastic scattering, within the framework of the Tassie model or models close to it, is a typical first stage of the reduction of the experimental data for the purpose of establishing the main characteristics of excited nuclei. (A brief survey of the data obtained by the Khar'kov group and their analysis are given in ref. 24, and some other studies are reviewed in ref. 69.)

On going to large q, or if a more detailed analysis of the experiment is needed, it is natural to use calculations with the radial transition density microscopic model. By way of example, we consider the analysis[36] of the ^{58}Ni nucleus. The charge-density distribution and the radial transition density of this nucleus were calculated in ref. 28 on the basis of Eq. (121). The results are shown in Figs. 27a and 28a. We see that the radial transition density has a characteristic maximum on the nuclear boundary (dashed curve). Averaging with the aid of Eq. (120) using the empirical nucleon charge density yields a smoother radial transition density (solid curve). The solid curve of Fig.

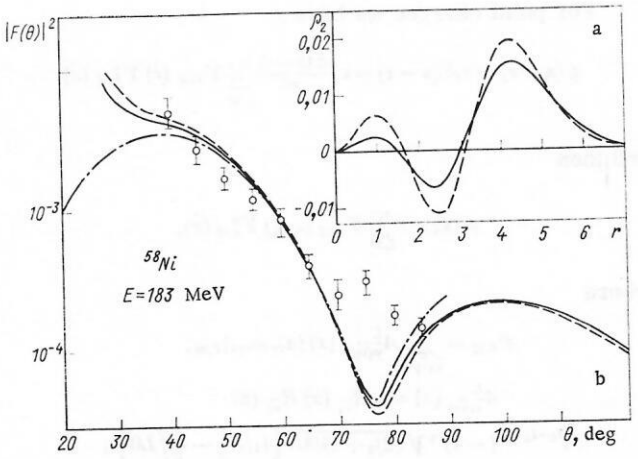

Fig. 27. Comparison of the exact (dash–dot curve) and approximate (using the high-energy approximation) calculations of inelastic scattering with excitation of the first 2^+ level in ^{58}Ni: The dashed and solid curves represent the "pointlike" and "smeared" transition densities calculated with a microscopic model in ref. 28, and the corresponding form factors.[36]

28 shows the charge-density distribution calculated in ref. 28 and reveals the predicted radial variations of this function, which are typical of the microscopic model and indeed distinguish it from the Fermi density (dashed curve). Following the procedure described above, we represent the function in the form of the series (103) and obtain by least squares the set $\{a_m^L\}$ of the coefficients. It turns out that at a sufficient accuracy of the fit (99%) it suffices to take only N = 10 terms of this series. Substituting the obtained set $\{a_m^L\}$ in relation (105) for the amplitude and next in expression (23) for the cross section, we obtain the final result, which is shown in Fig. 27b, where the form factor $|F|^2 = \sigma_{i \to f}/\sigma_{Mott}$ is plotted (the solid and dashed curves correspond to the transition densities shown in Fig. 27a). The dash–dot curve shows the exact calculations[28] with the transition density in the case of a "smeared" proton charge. It is seen that the proposed method results in good agreement (within the framework of the initial high-energy approximation, starting with $\vartheta = 40°$ and further) with the exact calculations.

We now analyze the latest experimental data on elastic scattering of electrons of energy E = 225 MeV by the nucleus ^{58}Ni (ref. 37), using the same charge and transition densities. Figure 28b shows the results of this analysis. The dashed curves represent calculations based on a hydrodynamic macroscopic model with the Fermi density ($R_0 = 4.148$, $b = 0.559$), while the solid curves correspond to the charge-density distributions and radial transition densities obtained in the microscopic model of ref. 28. Comparison with experiment shows that the calculated "microdensity" has too large a radius; this is manifest in a shift of the first elastic-scattering minimum towards smaller angles. What is more interesting is that both models yield a patently unsatisfactory description of the inelastic scattering in the region of the minimum, where the deviation from experiment reaches 70%.

In connection with the noted discrepancy, a model-independent search was undertaken for possible transition densities capable of adequately describing all the experimental inelastic-scattering points. In our approach, this task is easy, since the cross section (23) takes the

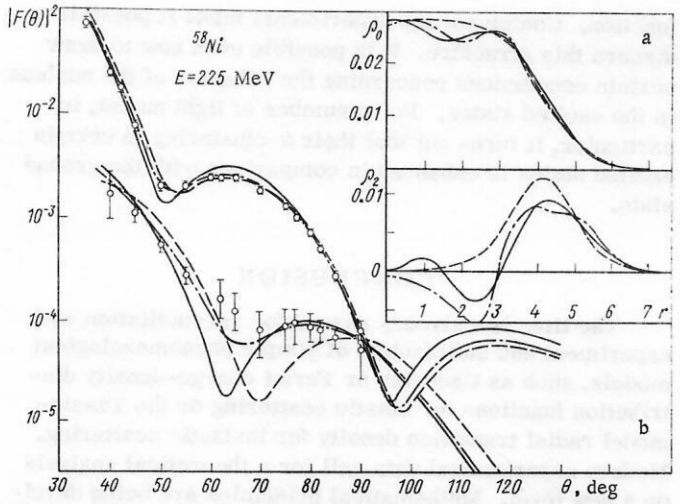

Fig. 28. Analysis of elastic and inelastic scattering of electrons with excitation of the first 2^+ level of ^{58}Ni. Dashed curves) calculation in macroscopic model with Fermi density; solid) calculation with microscopic model of ref. 28; dash–dot) one of the variants of the charge-density distribution and radial transition density, reconstructed from the elastic and inelastic form factors, respectively, by the method of model-independent analysis.[36]

form of a series of known functions having the same coefficients a_m as in the transition density (103). Therefore, through a χ^2 analysis of the experimental points, wherein these coefficients serve as variable parameters, it is possible to find one of the possible sets of a_m, and consequently also the corresponding transition density, which was normalized everywhere to the value of B(E2) so as to have $B(E2)/e^2 = |\int \rho_2(x)x^4dx|^2$ (the analysis has shown that the best value is $B(E2)/e^2 = 120$ F^2). The model-independent analysis was already used for elastic scattering; it was shown that from the available experimental data it is impossible to determine the charge-density distribution in the central part of the nucleus. In our case we obtain a similar result. The dash–dot curve in Fig. 28a shows one of the possible transition densities that yields good agreement with the experimental form factor, but differs significantly from the model radial transition densities in that it has a smoothed-out peak at the nuclear boundary and has a more complicated variation outside the nucleus. The result of an independent analysis for elastic scattering is shown in the same figure (dash–dot curve). A comparison of the curves obtained shows that the behavior of the transition density at the boundary of the nucleus does not coincide with the behavior of the derivative of the charge density, as postulated in the Tassie model. The last result may seem curious, for hitherto all the attempts to describe inelastic scattering were based mainly on macroscopic models, where this dependence was postulated from the very outset. A joint model-independent analysis of elastic and inelastic scattering was therefore carried out, in which this condition was also introduced, although the form of the initial charge-density distribution could be arbitrary, as shown above. The dash–dot curve of Fig. 13 show the results of this analysis. For comparison, the solid curves represent calculations corresponding to the usual approach on the basis of the Fermi density. The results show that the postulated connection between the charge-density distributions and the radial transition densities is a rather stringent condition and does not make it possible to describe inelastic scattering completely, in spite of the fact that there is a wide leeway in the variation of the density in the interior of the nucleus.

We consider now one more example, namely the results of an analysis of the inelastic form factors of the light nuclei ^{12}C and ^{16}O within the framework of Brink's α-cluster model. We derived above the corresponding expressions (93) for the charge-density distribution and the radial transition densities, and drew certain conclusions regarding the α-cluster properties of the ground states of a number of nuclei, properties that follow from elastic-scattering analysis. It turns out, in particular, that the clustering in ^{12}C is weak, and there is in fact no clustering in ^{16}O in the ground state. As to inelastic scattering, the analysis of refs. 48 and 52 leads to the following results: First, the calculations of the form factors of the rotational 2^+ and 3^- states of ^{12}C (ref. 48) with parameters corresponding to the best fit of elastic scattering (see Fig. 17) result in only qualitative agreement with experiment, mainly at small momentum transfers. Further, in either case it is impossible to obtain a set of parameters that describe equally well the elastic and inelastic scattering at all values of q. This is evidence that the approach in which the parameters of the α-cluster model with projection are assumed to be the same for all rotational-band states is of limited value.

It is therefore of interest to obtain an independent fit by varying the parameters of the trial functions of the form factors of the inelastic scattering with excitation of 2^+ and 3^- levels without any connection to the elastic-scattering parameters. This permits a detailed understanding of the structure of the excited states of the nucleus, e.g., their transition densities and the corresponding rms radii. Naturally, the fit should be based on trial functions with exponential asymptotic forms, so as to account for the region of the minimum of the inelastic form factor in the region $q \approx 2.5$–3.0 F^{-1}.

Figure 29 shows the results of such calculations and their comparison with experiment. First, it is seen from the figure that in this case, too, the ambiguity of the model comes into play, since at least three curves for each state can be regarded as in satisfactory agreement with experiment. A table of the corresponding parameters is given in ref. 52. Next, the rms nuclear radii, with fit parameters based on elastic scattering, turn out to be approximately 0.2 F larger than the corresponding elastic-scattering radii. A more interesting result, however, is for example the requirement that the best fit for inelastic scattering lead in the case of ^{12}C to the parameters R_α = 2.0 F and b_α = 0.5–0.6 F [$\overline{R}(^4\text{He}) = 1.77$–$1.9$ F]. They can be estimated in such a way that the α clusters in the excited states of ^{12}C become more compact than in the ground state, and have a tendency to approach the parameters of the free α particle. The same effect of cluster formation upon excitation of the nucleus is observed also in an analysis of the corresponding transition densities. Thus, for ^{12}C the transition densities with the best-fit parameters of the inelastic form factors are shifted much farther away from the center of the nucleus (by approximately 1 F) than those calculated with the parameters of the elastic scattering best fit. This is also confirmed by

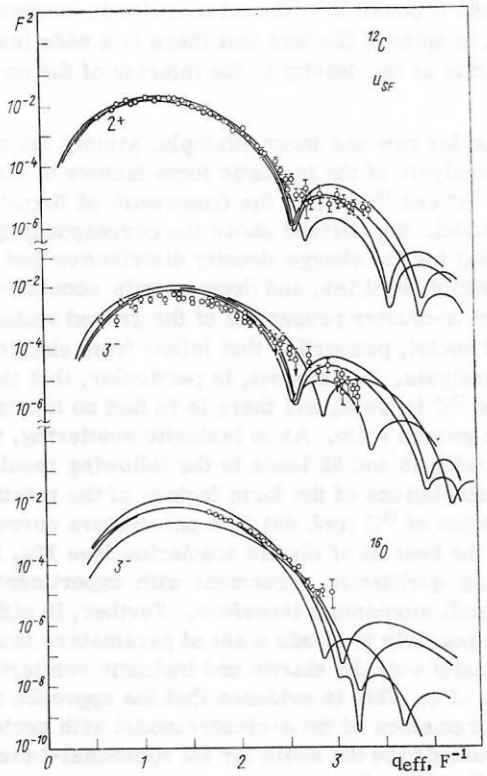

Fig. 29. Different variants of calculations of the inelastic form factors of ^{12}C and ^{16}O within the framework of the Brink α-cluster model with trial functions that are exponentially asymptotic.[52]

the change of the configuration parameter R. According to the elastic-scattering data, this parameter is much smaller than for the excited states.

The fact that the nuclear-structure parameters turn out to be different for different states indicates that the relation between the rotations and the oscillations plays an essential role. We note in this connection that an analysis of the form factors in the simple α-particle model with allowance for the possible α-cluster oscillations about their centers[70] extends the possibility of a unified description of an entire group of nuclear states.

Let us summarize our analysis of the inelastic scattering. Thus, the phenomenological approach itself yields much information on such important structural characteristics of the nucleus as the transition probabilities, the nuclear-shape parameters, etc. On the other hand, this approach is used also to establish the main geometrical characteristics of the region of the nucleus where the transition is concentrated. At small and medium q this region can be determined in accordance with the Tassie model, by relating the radial transition density with the derivative of the charge-density distribution. However, a detailed analysis of the experiment, including the region of large q, reveals that this relation is violated, and the radial transition density function must be specified independently. This function can be obtained with some degree of accuracy by using the methods of the model-independent analysis. But to understand the main features of the radial transition densities in the periphery of the nucleus (particularly if the nucleus is a medium or heavy one) it is important to make use of microscopic models, which yield the "fine structure" of the transition density function. Contemporary experiments make it possible to discern this structure. It is possible even now to draw certain conclusions concerning the behavior of the nucleus in the excited states. For a number of light nuclei, in particular, it turns out that their α clustering in certain excited states is enhanced in comparison with the ground state.

CONCLUSION

The time has already passed for reconciliation with experiment and satisfaction of simple phenomenological models, such as Gaussian or Fermi charge-density distribution functions for elastic scattering or the Tassie-model radial transition density for inelastic scattering. Modern experimental data call for a theoretical analysis on a new level. Mathematical principles are being developed for the method of model-independent analysis of the form factors, with an aim at extracting from the latter direct information on the true charge-density distribution and radial transition density functions of the nucleus. This is in essence a further development of the methods of the inverse scattering problem. As yet, the model independent analysis is incapable of singling out an unambiguous (of course, within the limits of some errors) charge-density distribution or radial transition density function that can be identified as the experimental function. In view of the limited amount of experimental information and in view of its own imperfection, this method is still incapable of getting rid of the ambiguities of the solutions. Much depends here on the choice of the form of the trial charge-density distribution and radial transition density functions, and on the additional information that can be introduced on the basis of other experiments. At the same time, nuclear-structure models are being perfected to make it possible to explain on the basis of a direct analysis not only the general qualitative laws governing the form factors, but also all the details of their behavior, especially at large momentum transfers.

It is obvious that the form factors are nuclear characteristics much more sensitive to various errors in the approaches and models than the "cruder" integral nuclear characteristics such as the energy or transition probability. Nonetheless, even here we encounter in the analysis of modern very precise data a rather curious situation. Indeed, a number of nuclear models give an approximately equally good description of the same experimental data after certain improvements are introduced in them. (We have purposely chosen the same data for the comparison, so as to illustrate this premise.) Thus, a direct model-dependent analysis does not make it possible to choose between the employed models solely on the basis of electron-scattering data. It is necessary to analyze the "justification" for the particular assumptions on which the models compared are based, using by way of tests additional data from other experiments. It is interesting that even within the framework of one model it is possible, by stretching things somewhat, to provide different explanations for the same set of form factors, although this is accomplished by changing the internal parameters of the model within "admissible" limits, so as not to violate the degree of agreement with other data. We have seen this with the α-cluster model of the nucleus as an example.

It can be concluded from all this that at the contemporary level of development of computer techniques, when practically any hypothesis can be readily fitted to the experimental data, one must be particularly careful to choose just scientific approaches and models, rather than speculative ones. Otherwise excessive faith in the illustration provided by any good fit to the experimental data can turn after some time into wasted effects exerted in the wrong direction.

In conclusion, the authors thank V. V. Burov for help in selecting and presenting the materials used in the review.

APPENDIX 1

Let us derive an expression for the functions $g(\mathbf{r}, \sigma)$ and $\phi(\mathbf{r})$ from (14) and (23) in explicit form. To this end, following ref. 7, we expand the Coulomb potential in a Taylor series and retain the quadratic term. For a spherically symmetrical distribution of the charge density $\rho(x)$ we have

$$V(r) = -4\pi\gamma \left\{ \frac{1}{r} \int_0^r \rho(x) x^2 dx + \int_r^\infty \rho(x)\, x\, dx \right\} \tag{A.1}$$

and

$$V(r) \approx V(0) + ak^3 r^2/2, \tag{A.2}$$

where

$$\gamma = Ze^2/(\hbar c) = Z/137;\ V(0) = -4\pi\gamma \int_0^\infty \rho(x)\, x\, dx;\ a = (4\pi/3)\,\gamma\rho(0)/k^3.$$

The first integral of the function (27) can then be evaluated by direct substitution of (A.2), while the second is estimated by expanding it in powers of the impact distance (ρ^2) and retaining the quadratic term

$$\phi^{(\pm)}(\mathbf{r}, \mathbf{k}) = -V(0)\cdot z - a\,(k^3\rho^2 z + k^3 z^2/3)/2 \mp b\,(\rho k)^2 + c\,(\rho k)^4, \tag{A.3}$$

where

$$b = \frac{\pi\gamma}{k^2} \int_0^\infty \rho(x)\, dx;\ c = -\frac{1}{8}\cdot\frac{\pi\gamma}{k^4} \int_0^\infty \frac{1}{x}\cdot\frac{d}{dx}\rho(x)\, dx.$$

Recognizing that $\mathbf{r} = \boldsymbol{\rho} + \hat{\mathbf{k}}z$ and $\boldsymbol{\rho} \perp \mathbf{k}$, we can rewrite (A.3) in the form

$$\phi^{(\pm)}(\mathbf{r}, \mathbf{k}) = -V(0)\,(\mathbf{kr})/k - \frac{1}{2}\,a\,(\mathbf{kr})\,(3k^2r^2 - 2\,(\mathbf{kr})) \mp b\,[\mathbf{rk}]^2 \pm c\,[\mathbf{rk}]^4. \tag{A.4}$$

Substituting (A.4) and (A.2) in (24) and (14) and confining ourselves to the terms linear in V(0), a, b, and c, we get

$$g(\mathbf{x}, \sigma) = (1 - V(0)/k)\,\{1 + a\,((\mathbf{k}_i\mathbf{x})^2 - [\mathbf{k}_i\mathbf{x}]^2 + (\mathbf{k}_f\mathbf{x})^2 - [\mathbf{k}_f\mathbf{x}]^2)$$
$$+ 3b\,((\mathbf{k}_i\mathbf{x}) - (\mathbf{k}_f\mathbf{x})) - 10c\,((\mathbf{k}_i\mathbf{x})\,[\mathbf{k}_i\mathbf{x}]^2 - (\mathbf{k}_f\mathbf{x})\,[\mathbf{k}_f\mathbf{x}]^2) - [a\,((\mathbf{k}_i\mathbf{x}) + (\mathbf{k}_f\mathbf{x}))/2$$
$$- 2c\,([\mathbf{k}_i\mathbf{x}]^2 - [\mathbf{k}_f\mathbf{x}]^2)](\sigma\mathbf{x})(1 - V(0)/k)\}; \tag{A.5}$$

$$\phi(\mathbf{x}) = -(\mathbf{k}_i - \mathbf{k}_f)\,\mathbf{x}\,[V(0)/k] - a\,(3k^2x^2\,(\mathbf{k}_i\mathbf{x} - \mathbf{k}_f\mathbf{x}) - 2\,(\mathbf{k}_i\mathbf{x})^3$$
$$+ 2\,(\mathbf{k}_f\mathbf{x})^3)/2 - b([\mathbf{xk}_i]^2 + [\mathbf{xk}_f]^2) + c\,([\mathbf{xk}_i]^4 + [\mathbf{xk}_f]^4). \tag{A.6}$$

We choose the axis $\mathbf{oz} \uparrow\uparrow \mathbf{q}$, where $\mathbf{q} = \mathbf{k}_i - \mathbf{k}_f = 2k\sin\vartheta/2 = 2k\alpha$, $\alpha = \sin\vartheta/2$, and the axis $\mathbf{ox} \perp \mathbf{q}$. Then $\cos(\hat{\mathbf{q}}\hat{\mathbf{x}}) = \mu$, $\mathbf{x} = \{x\mu\varphi\}$;

$$\cos\hat{x}\,\hat{k}_i = \mu\alpha + \sqrt{1-\mu^2}\,\sqrt{1-\alpha^2}\cos\varphi;$$
$$\cos\hat{x}\,\hat{k}_f = -\mu\alpha + \sqrt{1-\mu^2}\,\sqrt{1-\alpha^2}\cos\varphi.$$

Taking into account this fact and $|\mathbf{k}_i| = |\mathbf{k}_f| = k$, we obtain for $\mu = \varepsilon = \pm 1$

$$g(x\mu\varphi)|_{\mu=\varepsilon} = g(x, \varepsilon) = (1 - V(0)/k)^2\cdot\{1 + \varepsilon b 3qx + a\,(q^2 - 2k^2)\,x^2$$
$$- 5\varepsilon cq\,(4k^2 - q^2)\,x^3/2\}; \tag{A.7}$$

$$\phi(x\mu\varphi)|_{\mu=\varepsilon} = \phi(x, \varepsilon) = -\varepsilon V(0)qx/k - b\,(4k^2 - q^2)\,x^2/2 - \varepsilon a\,(qk^2/2$$
$$- q^3/12)\,x^3 + c\,(4k^2 - q^2)\,x^4/8. \tag{A.8}$$

Let us find also an expression for $q_{\text{eff}}(x, \varepsilon)$ and $D(x, \varepsilon, \varphi)$:

$$q_{\text{eff}}(x\mu\varphi)|_{\mu=\varepsilon} = q_{\text{eff}}(x\varepsilon) = \varepsilon q\,(1 - V(0)/k) - \varepsilon aq\,(3k^2/2 - q^2/4)\,x^2$$
$$- b\,(4k^2 - q^2)\,x + c\,(4k^2 - q^2)^2\,x^3/2; \tag{A.9}$$

$$qxD(x\varepsilon\varphi) = qx + \frac{\partial}{\partial\mu}\,\phi(x\mu\varphi)|_{\mu=\varepsilon} = A(x, \varepsilon) + B(x, \varepsilon)\cos^2\varphi; \tag{A.10}$$

$$A(x\varepsilon) = qx\,(1 - V(0)/k) - a\,(k^2q^2/2 - q^3/4)\,x^3 + \varepsilon bq^2x^2 - \varepsilon cq^2/2\,(4k^2 - q^2)\,x^4; \tag{A.11}$$

$$B(x\varepsilon) = -aq/2\,(4k^2 - q^2)\,x^3 - \varepsilon b\,(4k^2 - q^2)\,x^2 + \varepsilon c\,(2k^2 - 3q^2/2)\,(4k^2 - q^2)\,x^4. \tag{A.12}$$

APPENDIX 2

In the calculation of $G_{LM}(x, \varepsilon)$ in (31) we encounter integrals of the type

$$\int_0^{2\pi} \frac{\cos M\varphi}{[A + B\cos^2\varphi]^\nu}\, d\varphi, \tag{A.13}$$

which differ from zero only at even M: M = 2m. Using

$$\cos 2m\varphi = \sum_{n=0}^{m} (-1)^n\, C_{2n}^{2m} \cos^{2m-2n}\varphi\, \sin^{2n}\varphi \tag{A.14}$$

and making the substitution $\varphi \to \varphi + \pi/2$, we arrive at the integral[12]

$$\int_0^{\pi/2} \frac{\sin^n\varphi\cos^m\varphi}{[(A+B) - B\cos^2\varphi]^\nu}\, d\varphi$$
$$= \frac{1}{2\,(A+B)^\nu}\, B\left(\frac{n+1}{2}, \frac{m+1}{2}\right) F\left(\frac{m+1}{2}, \nu, \frac{m+n}{2} + 1; Z\right), \tag{A.15}$$

where the hypergeometric function $F(\alpha, \beta, \gamma, Z)$ is expressed in the form of a series in $Z = B/(A + B)$.

We present several expressions for $G_{LM}(x, \varepsilon)$:

$$G_{00} = \frac{qxg(x, \varepsilon)}{\sqrt{A(x, \varepsilon)\,[A(x, \varepsilon) + B(x, \varepsilon)]}}\cdot\frac{1}{\sqrt{4\pi}};$$
$$G_{10} = G_{00}\sqrt{3}\,[\varepsilon + i\,(1 - Z/2)/A];$$
$$G_{20} = G_{00}\sqrt{5}\,[1 + i3\varepsilon\,(1 - Z/2)/A - 3\,(1 - Z + 3Z^2/8)/A^2];$$
$$G_{2\pm2} = \sqrt{30}\,G_{00}\,[i\varepsilon\,(Z - 3Z^2)/A - (3Z/2 - 15Z^2/2)/A^2]/4;$$
$$G_{30} = G_{00}\sqrt{7}\,[\varepsilon + i6\,(1 - Z/2)/A - 15\varepsilon\,(1 - Z + 3Z^2/8)/A^2 -$$
$$- i15\,(1 - 3Z/2 + 9Z^2/8)/A^3];$$
$$G_{3\pm2} = \sqrt{210}\,G_{00}\,[i\,(Z - 3Z^2)/A - 3\varepsilon\,(3Z/4 - 15Z^2/4)/A^2 - i3\,(Z - 7Z^2)/A^3]/4.$$

---

[1] H. Uberall, Electron Scattering from Complex Nuclei, Academic Press, New York (1971).

[2] Yu. S. Pol', V. K. Luk'yanov (Lukyanov), and I. Zh. Petrov, Acta Phys. Pol., 34, 49 (1968).

[3] R. J. Glauber, Lectures in Theoretical Physics, Vol. 1, New York (1959), p. 315.

[4] A. Baker, Phys. Rev. B, 234, 240 (1964).

[5]L. I. Schiff, Phys. Rev., 103, 443 (1956).
[6]J. J. Tiemann, Phys. Rev., 109, 183 (1958).
[7]D. R. Yennie, F. L. Boos, and D. G. Ravenhall, Phys. Rev. B, 137, 882 (1965).
[8]I. Zh. Petkov, V. K. Luk'yanov, and Yu. S. Pol', Yad. Fiz., 4, 57 (1966) [Sov. J. Nucl. Phys., 4, 41 (1967)].
[9]V. K. Luk'yanov, I. Zh. Petkov, and Yu. S. Pol', Yad. Fiz., 9, 349 (1969) [Sov. J. Nucl. Phys., 9, 204 (1969)].
[10]R. Herman, B. C. Clark, and D. G. Ravenhall, Phys. Rev., 132, 414 (1963).
[11]Yu. N. Eldyshev, V. K. Luk'yanov, and Yu. S. Pol', Yad. Fiz., 16, 506 (1972) [Sov.J. Nucl. Phys., 16, 282 (1973)].
[12]I. S. Gradshtein and I. M. Ryzhik, Tables of Integrals, Sums, Series, and Products [in Russian], Fizmatgiz (1962).
[13]R. F. Frosch et al., Phys. Rev., 160, 874 (1967).
[14]G. C. Li et al., Nucl. Phys. A., 162, 583 (1970).
[15]I. Sick and J. S. McCarthy, Nucl. Phys. A, 150, 631 (1970).
[16]J. B. Bellicard et al., Phys. Rev. Lett., 19, 9 (1967).
[17]B. Hahn, R. Hofstadter, and D. G. Ravenhall, Phys. Rev., 105, 1353 (1957).
[18]R. Hofstadter et al., Phys. Rev. Lett., 15, 758 (1965).
[19]K. J. Van Oostrum et al., Phys. Rev. Lett., 16, 528 (1966).
[20]R. F. Frosch et al., Phys. Rev., 174, 1380 (1968).
[21]V. M. Khvastunov et al., Yad. Fiz., 10, 217 (1969)[Sov. J. Nucl. Phys., 10, 122 (1970)]; Nucl. Phys. A., 146, 15 (1970).
[22]A. S. Litvinenko et al., Yad. Fiz., 14, 40 (1971)[Sov. J. Nucl. Phys., 14, 23 (1972)].
[23]A. S. Litvinenko et al., Yad. Fiz., 14, 479 (1971)[Sov. J. Nucl. Phys., 14, 269 (1972)].
[24]N. G. Afanas'ev et al., in: Proceedings, Fourth Intern. Conf. on High Energy Physics and Nuclear Structure [in Russian], Dubna (1971).
[25]G. D. Alkhazov, Preprint 48, Leningrad Inst. Nucl. Phys. (1973).
[26]G. C. Li, I. Sick, and M. R. Yearian, Phys. Lett. B, 37, 282 (1971); HEPL Preprint No. 691, Stanford (1973).
[27]J. Heisenberg et al., Phys. Rev. Lett., 23, 1402 (1969).
[28]I. T. Reynolds and D. S. Onley, Nucl. Phys., 66, 1 (1965).
[29]A. N. Tikhonov, Dokl. Akad. Nauk SSSR, 151, 501 (1963); 153, 49 (1963).
[30]Yu. S. Pol', Yad. Fiz., 10, 771 (1969)[Sov. J. Nucl. Phys., 10, 445 (1970)].
[31]M. Groissiaux et al., Phys. Rev. B., 137, 865 (1965).
[32]J. B. Bellicard et al., Phys. Rev. Lett., 19, 527 (1967).
[33]H. H. Wolter, A. Faessler, and P. U. Sauer, Nucl. Phys. A., 116, 145 (1968).
[34]J. Friedrich and F. Lenz, Nucl. Phys. A., 183, 523 (1972).
[35]J. L. Frian and J. W. Negele, Nucl. Phys. A, 212, 93 (1973).
[36]V. K. Luk'yanov and Yu. S. Pol', Yad. Fiz., 11, 556 (1970)[Sov. J. Nucl. Phys., 11, 312 (1970).
[37]V. M. Khvastunov et al., Phys. Lett. B, 28, 119 (1968); V. D. Afanas'ev et al., Ukr. Fiz. Zh., 13, 1919 (1968), Yad. Fiz., 10, 33 (1969)[Sov. J. Nucl. Phys. Phys., 10, 18 (1970)].
[38]V. M. Strutinskii, in: Nuclear Structure (Lectures, Alushta School) [in Russian], D-6465 (1972), p. 467.
[39]P. É. Nemirovskii, Yad. Fiz., 7, 53 (1968)[Sov. J. Nucl. Phys., 7, 38 (1968)].
[40]Yu. S. Pol', Program and Abstracts, 19-th Conf. On Nucl. Spectroscopy and Nuclear Structure, Erevan [in Russian], Nauka (1969).
[41]N. G. Afanas'ev et al., Yad. Fiz., 8, 1112 (1968)[Sov. J. Nucl. Phys., 8, 646 (1969)].
[42]T. de Forest and J. D. Walecka, Adv. Nuc. Phys., 15, No. 57 (1966), p. 1.
[43]G. C. Li, I. Sick, and M. R. Yearian, HEPL-691 (1973).
[44]B. Castel et al., Nucl. Phys. A, 157, 137 (1970).
[45]V. G. Neudachin and Yu. F. Smirnov, Nucleon Clusters in Light Nuclei [in Russian], Nauka (1969).
[46]E. V. Inopin and B. I. Tishchenko, Zh. Eksp. Teor. Fiz., 38, 1160 (1960) [Sov. Phys.-JETP, 11, 840 (1969)]; E. V. Vadia, E. V. Inopin, and M. Yusef, Zh. Eksp. Teor. Fiz., 45, 1164 (1963)[Sov. Phys.-JETP, 18, 802 (1964)]; E. V. Inopin, A. A. Kresnin, and B. I. Tishchenko, Yad. Fiz., 2, 802 (1965)[Sov. J. Nucl. Phys., 2, 573 (1966)].
[47]D. M. Brink, in: Structure of Complex Nuclei [Russian translation], Atomizdat (1966), p. 111; D. M. Brink, "Enrico Fermi" Intern. School of Physics, Course XXXVI (1965); D. M. Brink et al., Phys. Lett. B, 33, 143 (1970).
[48]E. V. Ionopin, V. K. Luk'yanov, and Yu. S. Pol', Yad. Fiz., 19, 987 (1974) [Sov. J. Nucl. Phys., 19, 507 (1974)]; E. V. Inopin, V. K. Luk'yanov, and Yu. S. Pol', Proc. Intern. Conf. Nucl. Phys., Munich, 1973, Vol. 1, p. 617.
[49]R. E. Peierls and J. Yoccoz, Proc. R. Soc. A, 70, 381 (1970).
[50]I. Sh. Vashakidze and T. R. Dzhalaganiya, Yad. Fiz., 16, 941 (1971) [Sov. J. Nucl. Phys., 16, 519 (1972)]; N. Takigawa and A. Arima, Nucl. Phys. A, 168, 593 (1971).
[51]P. S. Hauge, S. A. Williams, and G. H. Duffey, Phys. Rev., C4, 1044 (1971); L. J. McDonald, H. Uberall, and S. Numrich, Nucl. Phys., A 147, 541 (1970).
[52]E. V. Inopin et al., JINR Preprint R4-7741 (1974).
[53]W. Czyz and L. Lesniak, Phys. Lett., 25B, 319 (1967).
[54]R. Jastrow, Phys. Rev., 98, 1479 (1955).
[55]C. Ciofi degli Atti, Nucl. Phys., A129, 350 (1969).
[56]A. Malecki and P. Picchi, Riv. Nuovo Cimento, 2, 119 (1970); Lett. Nuovo Cimento, 1, 41 (1971).
[57]C. Ciofi degli Atti and N. M. Kabachnik, Phys. Rev., C1, 809 (1970).
[58]F. Iwamoto and H. Yamada, Progr. Theor. Phys., 17, 543 (1957).
[59]T. H. R. Skyrme, Phil. Mag., 1, 1043 (1956); Nucl. Phys., 9, 615 (1959).
[60]D. Vautherin and D. M. Brink, Phys. Rev., C5, 626 (1972).
[61]W. F. Ford, R. C. Braley, and J. Bar-Touv, Phys. Rev., C4, 2099 (1971).
[62]L. J. Tassie, Austral. J. Phys., 9, 407 (1956).
[63]D. Brink and G. Satchler, Angular Momentum, Oxford (1962).
[64]I. Zh. Petkov, V. K. Luk'yanov, and Yu. S. Pol', Yad. Fiz., 4, 556 (1966) [Sov. J. Nucl. Phys., 4, 395 (1967)].
[65]J. Bellicard, P. Barreau, and D. Blum, Nucl. Phys., 60, 319 (1964).
[66]W. Bertozzi et al., Phys. Rev. Lett., 28, 1711 (1972).
[67]I. Zh. Petkov, V. K. Luk'yanov, and Yu. S. Pol', JINR Preprint R-2490, Dubna (1965).
[68]V. K. Luk'yanov and I. Zh. Pertkov, Izv. AN SSSR, Ser. Fiz., 28, 1207
[69]T. DeForest, in: Electromagnetic Interactions of Nuclei at Low and Medium Energies [in Russian], Nauka (1973).
[70]A. N. Antonov and E. V. Inopin, Yad. Fiz., 16, 326 (1972) [Sov. J. Nucl. Phys., 16, 182 (1973)].